

Defining a quantum active particle using a non-unitary quantum walk

Manami Yamagishi*

*Department of Physics, the University of Tokyo, 5-1-5 Kashiwanoha, Kashiwa, Chiba 277-8574, Japan and
Theoretical Quantum Physics Laboratory, Cluster for Pioneering Research,
RIKEN, 2-1 Hirosawa, Wako, Saitama 351-0198, Japan*

Naomichi Hatano†

*Institute of Industrial Science, the University of Tokyo,
5-1-5 Kashiwanoha, Kashiwa, Chiba 277-8574, Japan*

Hideaki Obuse‡

*Department of Applied Physics, Hokkaido University, Kita 13,
Nishi 8, Kita-Ku, Sapporo, Hokkaido 060-8628, Japan and
Institute of Industrial Science, the University of Tokyo,
5-1-5 Kashiwanoha, Kashiwa, Chiba 277-8574, Japan*

(Dated: September 11, 2023)

The main aim of the present paper is to define an active matter in a quantum framework and investigate difference and commonalities of quantum and classical active matters. Although the research field of active matter has been expanding wider and wider, most research is conducted in classical systems. We here propose a truly deterministic quantum active-matter model with a non-unitary quantum walk as minimal models of quantum active matter in one- and two-dimensional systems. We aim to reproduce similar results that Schweitzer *et al.* [1] obtained with their classical active Brownian particle; that is, the Brownian particle, with a finite energy take-up, becomes active and climbs up a potential wall. We realize such a system with non-unitary quantum walks. We introduce new internal states, the ground state $|G\rangle$ and the excited state $|E\rangle$, and a new non-unitary operator $N(g)$ for an asymmetric transition between $|G\rangle$ and $|E\rangle$. The non-Hermiticity parameter g promotes transition to the excited state and hence the particle takes up energy from the environment. We realize a system without momentum conservation by manipulating a parameter θ for the coin operator for a discrete-time quantum walk; we utilize the property that the continuum limit of a one-dimensional discrete-time quantum walk gives the Dirac equation with its mass proportional to the parameter θ [2]. With our quantum active particle, we successfully observe that the movement of the quantum walker becomes more active in a non-trivial way as we increase the non-Hermiticity parameter g , which is similar to the classical active Brownian particle [1]. Meanwhile, we also observe three unique features of quantum walks, namely, ballistic propagation of peaks in one dimension, the walker staying on the constant energy plane in two dimensions, and oscillations originating from the resonant transition between the ground state $|G\rangle$ and excited state $|E\rangle$ both in one and two dimensions.

I. INTRODUCTION

Active matter is a self-driven component or a collection of such components [3]. Active matter can be un-living matters as well as living ones like birds and fish. From a physical point of view, an active matter takes up energy from the environment, stores it inside, converts the internal energy into kinetic energy, and thereby moves (Fig. 1). The active Brownian particle [4], which appears in the following sections, is a prototypical example of active matter.

The research area of active matter is highly interdisciplinary; it extends over biology [5, 6], chemistry [7], and physics [8]. Introduction of the idea of active matter enabled us to unify a variety of studies which had been investigated separately before and to understand their commonalities and universalities [9]. Starting from the models proposed by Vicsek [10] and Toner and Tu [11] separately in 1995, theoret-

ical studies have lead the research of classical active matter. Various phenomena unique to active matter have been found, *e.g.* true long-range order [10], giant number fluctuation (GNF) [12, 13] and motility-induced phase separation (MIPS) [14, 15]. A recent research [16] connecting classical active matter and topological phenomena, such as the Hall effect, is gathering much attention. These studies have attracted and fascinated many researchers, and now that more and more models are realized in experiments [17–21], the research field has been expanding wider and wider.

However, most research is conducted in classical systems. There are few works that tried to introduce the concept of active matter into quantum systems. Adachi *et al.* [22] modeled a many-body version of quantum active matter, connecting a classical stochastic active matter to a non-Hermitian quantum spin systems, which they referred to a “stoquastic” Hamiltonian; Zheng and Löwen [23] used a quantum harmonic oscillator with its potential minima externally driven by stochastic active dynamics. The authors of the former paper recently considered another model in one dimension [24] based on their first model [22], finding a flocking phase as ferromagnetism of a quantum spin model. There is recently another

* manami@iis.u-tokyo.ac.jp

† hatano@iis.u-tokyo.ac.jp

‡ hideaki.obuse@eng.hokudai.ac.jp

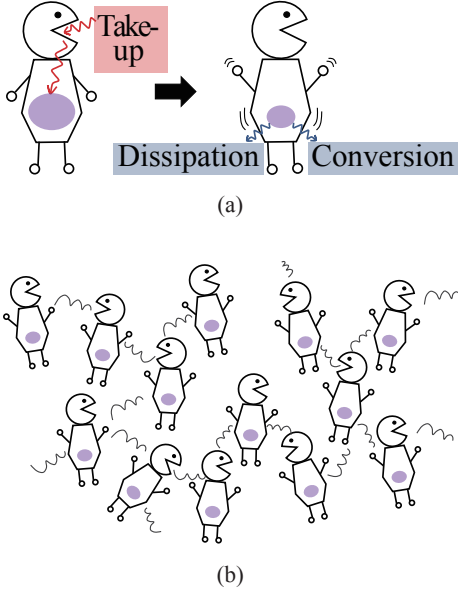


FIG. 1: Schematic views of active matter. (a) A component that takes up energy from the environment, stores it inside, converts the stored internal energy to the kinetic energy and moves, or (b) an interacting collection of such components.

TABLE I: Classification of systems without energy conservation. Studying quantum active matter enables us to extend non-Hermitian physics to systems without momentum conservation and to extend classical active matter to quantum systems.

	Momentum conserved	Momentum not conserved
Classical	Dissipative systems	Classical active matter
Quantum	Non-Hermitian physics	Quantum active matter

work on active quantum flocks [25] by Khasseh *et al.*

In the present paper, we define a quantum active matter using discrete-time quantum walks[26–30]. Since the quantum walk does not have any stochasticity of classical random walks and does not have any classical limits, neither does our model.

We have in our mind the diagram shown in Table I. We believe that the following two points are essential properties for a system to be an active matter:

- (i) neither energy nor momentum are conserved;
- (ii) the kinetic motion depends on particles' internal states.

The energy non-conservation results in temporally inhomogeneous dynamics, such as decay and growth, whereas the momentum non-conservation, which is equivalent to the breakdown of the law of action and reaction, results in spatially inhomogeneous dynamics, such as a pair of birds meeting up

and flying along together. We would define distinctive universality classes of quantum active matter by updating non-Hermitian, energy non-conservative quantum models into the new realm of momentum non-conservation.

In this paper, trying to find a minimal model of quantum active matter, we define a one-particle non-Hermitian quantum system that exhibits real-time evolution in a fully quantum range without external manipulation as in Ref. [23]. In our quantum active-matter model, internal states that are strongly correlated with the environment dominate the system dynamics. Strong correlation with the environment makes the system open and non-Hermitian, without energy conservation. We note that the non-Hermiticity of our model Hamiltonian belongs to the class of so-called pseudo-Hermiticity [31–33], because of which all energy-like eigenvalues of the unitary dynamics are real, although the energy expectation values are not conserved. It never exhibits Markovian decays due to complex eigenvalues of non-Hermitian Hamiltonians that one would find in the Gorini-Kosakowski-Sudarshan-Lindblad equation [34, 35] under postselection of no quantum jumps [36–42]. One notable point of our model is that we break the momentum conservation deliberately. Hence our system evolves differently from the cases of ordinary non-Hermitian quantum mechanics.

A. Classical active Brownian Particle

Let us next review a previous research on a prototypical classical active Brownian particle [1]. This model may differ from major ones in the context of studies on active matter [43–45]. However, the authors of the study that we review here made the correspondence between the internal energy of the particle and its dynamics very clearly, which is why we chose this study to start with. Schweitzer *et al.* [1] studied the dynamics of a Brownian particle with ability to take up energy from the environment, store it inside, convert the internal energy into kinetic energy and move. In order to model the dynamics, they added a new term of the internal energy $e(t)$ to the right-hand side of the Langevin equation. They first studied dynamics of an active Brownian particle under a harmonic potential with a constant energy take-up. The active Brownian particle moved almost on a limit cycle with a finite energy take-up, whereas a simple Brownian particle without an energy take-up did not. We aim to reproduce similar results to theirs: a quantum particle moves around more actively, climbing up the harmonic potential with a finite energy take-up. At the same time, we aim to observe its quantum features not present in its classical counterpart. In order to achieve them, we use non-unitary quantum walks[46–48] as a tool.

B. Quantum walks

The quantum walk is a quantum analogue of random walk. Nonetheless, note that the quantum walk exhibits distinctively quantum dynamics, without any stochasticity. Instead of stochastic fluctuations of the classical random walker, the

quantum walker moves under quantum interference at each site, which deterministically governs the dynamics of the walker's wave function. Its classical limit might be possible only after introducing decoherence or other additional effects.

Quantum walk was originally introduced by Aharonov *et al.* [26], who first referred to it as “quantum random walk”. Meyer [27] built a systematic model and found a correspondence to Feynman's path integral [49] of the Dirac equation. Started by Farhi and Gutmann [28], quantum walks have been well studied in the context of quantum information [29, 30]. To this day, studies of quantum walks have become even more interdisciplinary and extended over a variety of research fields, such as biophysics [50, 51] and condensed-matter physics [52], particularly topological materials [53–56].

There are two types of time evolution: continuum-time quantum walks and discrete-time quantum walks. In the present paper, we focus on the latter, in which the space and time are both discrete. In Sec. II, we first investigate non-unitary quantum walk as a quantum active particle in one dimension. In need of extension of our quantum active matter to higher dimensions, we utilize in Sec. III multi-dimensional quantum walks [57] with which we can make correspondence to the Dirac equation and further to the Schrödinger equation in higher dimensions. Section. IV summarizes the paper. To make the paper self-contained, we provide a compact review of the quantum walk in Appendix A.

II. QUANTUM ACTIVE PARTICLE IN ONE DIMENSION

A. One-dimensional model

In one dimension, our quantum active particle has four internal states in total, namely, $(|L\rangle \oplus |R\rangle) \otimes (|G\rangle \oplus |E\rangle)$. Here, $|L\rangle$ and $|R\rangle$ denote the leftward and rightward states, respectively, while $|G\rangle$ and $|E\rangle$ denote the ground and excited states, respectively. We define the time evolution of our one-dimensional quantum active particle $|\psi(T)\rangle = [U^{(1)}(g)]^T |\psi(0)\rangle$ for $T \in \mathbb{Z}$ in terms of the following operators:

$$N^{(1)}(g) := \sum_x \left[|x\rangle\langle x| \otimes e^{-iH_{\text{NH}}^{(1)}(g)} \right], \quad (1)$$

$$C^{(1)} := \sum_x \left[|x\rangle\langle x| \otimes e^{-iH_C^{(1)}(x)} \right], \quad (2)$$

$$S^{(1)} := \sum_x \left[|x-a\rangle\langle x| \otimes |L\rangle\langle L| + |x+a\rangle\langle x| \otimes |R\rangle\langle R| \right], \quad (3)$$

with $U^{(1)}(g) := SCN^{(1)}(g)$ and with the lattice constant a . Here,

$$H_{\text{NH}}^{(1)}(g) := \left(\begin{array}{cc|cc} -\varepsilon & 0 & -we^{-g} & 0 \\ 0 & -\varepsilon & 0 & -we^{-g} \\ \hline -we^{+g} & 0 & +\varepsilon & 0 \\ 0 & -we^{+g} & 0 & +\varepsilon \end{array} \right), \quad (4)$$

$$H_C^{(1)}(x) := \left(\begin{array}{cc|cc} 0 & -i\theta_G(x) & 0 & 0 \\ i\theta_G(x) & 0 & 0 & 0 \\ \hline 0 & 0 & 0 & -i\theta_E(x) \\ 0 & 0 & i\theta_E(x) & 0 \end{array} \right), \quad (5)$$

$$|L\rangle\langle L| = \begin{pmatrix} 1 & 0 & 0 & 0 \\ 0 & 0 & 0 & 0 \\ 0 & 0 & 1 & 0 \\ 0 & 0 & 0 & 0 \end{pmatrix}, \quad |R\rangle\langle R| = \begin{pmatrix} 0 & 0 & 0 & 0 \\ 0 & 1 & 0 & 0 \\ 0 & 0 & 0 & 0 \\ 0 & 0 & 0 & 1 \end{pmatrix}. \quad (6)$$

We used the bases $\{|L\rangle \otimes |G\rangle, |R\rangle \otimes |G\rangle, |L\rangle \otimes |E\rangle, |R\rangle \otimes |E\rangle\}$ in this order to represent the matrices. In Eq. (4), $\mp\varepsilon$ denotes the levels of $|G\rangle$ and $|E\rangle$, respectively, while the non-Hermitian parameter g specifies the difference in the transitions between the two levels. The non-Hermiticity of $H_{\text{NH}}^{(1)}$ makes the total time-evolution operator $U^{(1)}(g)$ non-unitary. We can interpret the non-Hermiticity of $H_{\text{NH}}^{(1)}$ as an effect of laser pumping; see Sec. II B. Note that the energy conservation is broken because of our non-Hermitian Hamiltonian $H_{\text{NH}}^{(1)}(g)$. Thus it satisfies the first half of the property (i) of quantum active matter; the energy is not conserved. In fact, we will show below in Eq. (8) that the Hamiltonian (4) has a symmetry called the pseudo-Hermiticity [31–33], and hence the energy eigenvalues remain real, not depending on g at all, but the energy expectation value are not conserved.

In Eq. (5), we set the parameter for the excited state $\theta_E(x)$ generally less than that of the ground state $\theta_G(x)$. This is because of the following reason. The continuum limit of the unitary time evolution of one-dimensional [2] and two-dimensional [57] quantum walks yields a Dirac Hamiltonian with the parameters for the coin operator θ of the former being proportional to the mass terms of the latter. We set $\theta_E < \theta_G$ so that we can make our quantum active particle run faster in the excited state than in the ground state. In other words, our active quantum walker does not conserve the momentum, which is the second half of the property (i) of quantum active matter; the momentum is not conserved either. Since it runs faster when pumped from the ground state to the excited state, it also satisfies the property (ii) of quantum active matter; the kinetic motion depends on particles' internal states. See Fig. 2 for details of the time evolution.

One notable point is that we can make the non-Hermitian matrix $H_{\text{NH}}^{(1)}(g)$ Hermitian with a similarity transformation called the imaginary gauge transformation [58, 59]

$$A(g) = \text{diag}(e^{-g/2}, e^{-g/2}, e^{+g/2}, e^{+g/2}) \quad (7)$$

as in

$$\begin{aligned} A(g)^{-1} H_{\text{NH}}^{(1)}(g) A(g) &= A(-g) H_{\text{NH}}^{(1)}(g) A(g) \\ &= \left(\begin{array}{cc|cc} -\varepsilon & 0 & -w & 0 \\ 0 & -\varepsilon & 0 & -w \\ \hline -w & 0 & +\varepsilon & 0 \\ 0 & -w & 0 & +\varepsilon \end{array} \right) \\ &= H_{\text{NH}}^{(1)}(g=0). \end{aligned} \quad (8)$$

In other words, the eigenvalues of our Hamiltonian (4) remain real for any values of the non-Hermiticity parameter

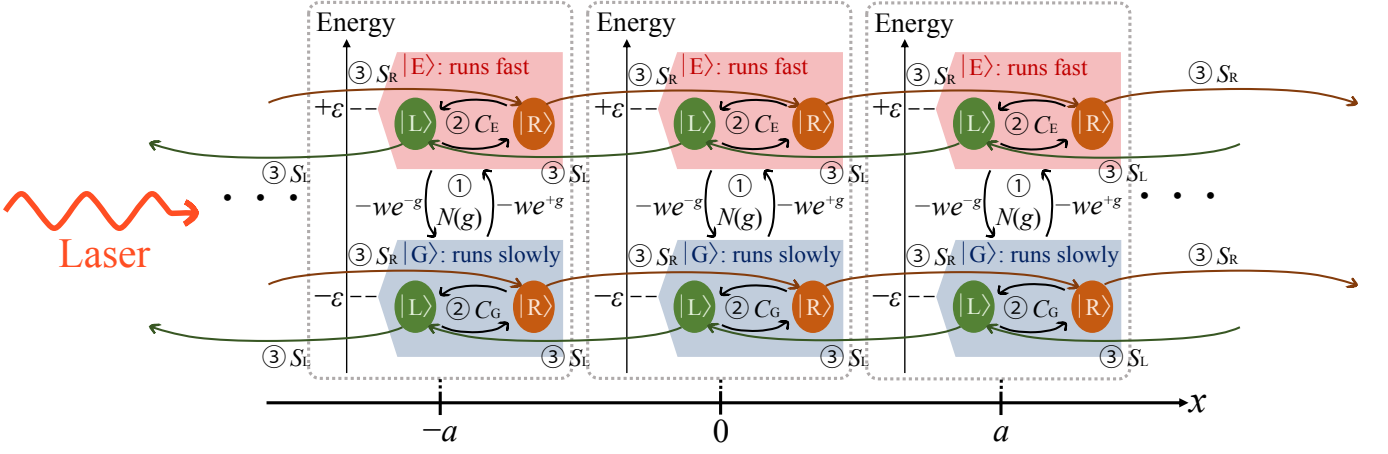


FIG. 2: Time evolution of our quantum active particle in one dimension. There are four internal states, namely, $(|L\rangle \oplus |R\rangle) \otimes (|G\rangle \oplus |E\rangle)$ at each site. The parameters ε , w and g are all real. We have the coin operator (②), the shift operator (③), and the new operator for asymmetric transition between the ground state $|G\rangle$ and the excited state $|E\rangle$, which describes energy take-up (①). We use different θ for the ground state $|G\rangle$ and the excited state $|E\rangle$ to realize a system without momentum conservation.

g . This property is often called pseudo-Hermiticity [31–33]. In this sense our non-Hermitian Hamiltonian (4) is distinct from non-Hermitian Hamiltonians that one would find in the Gorini-Kosakowski-Sudarshan-Lindblad equation [34, 35] under postselection of no quantum jumps [36–42], which can have complex eigenvalues that describe Markovian decays.

Note also that both $S^{(1)}$ and $C^{(1)}$ commute with $A(g)$; the matrix $A(\pm g)$ consists of two blocks for the ground and excited states, each of which is just the identity matrix multiplied by either $e^{\pm g/2}$, while the matrices $S^{(1)}$ and $C^{(1)}$ also consist of two blocks. Therefore the total time-evolution operator $U(g)$ can be also transformed to $U^{(1)}(0)$ as in

$$\begin{aligned} A(g)^{-1}U^{(1)}(g)A(g) &= A(g)^{-1}S^{(1)}C^{(1)}N^{(1)}(g)A(g) \\ &= S^{(1)}C^{(1)}\left[A(g)^{-1}N^{(1)}(g)A(g)\right] = S^{(1)}C^{(1)}N^{(1)}(0) \\ &= U^{(1)}(0). \end{aligned} \quad (9)$$

Therefore the eigenvalues of the non-unitary matrix $U^{(1)}(g)$ are identical to those of the unitary matrix $U^{(1)}(g=0)$, which are located on the unit circle in the complex plane (see Fig. 3). We can call this the pseudo-unitarity [60]. The same applies to the two-dimensional case, which we describe in Sec. III A. We thereby refer to our dynamics as purely deterministic quantum dynamics.

Nevertheless, the total probability and the energy expectation value are not conserved because the eigenvectors of $U^{(1)}(g)$ are not orthogonal to each other. Since we use the right-eigenvector and its Hermitian conjugate to calculate the probability density $P(x, T)$ as in Eq. (19) below as well as expectation values, there remain fluctuations of the probability density and the energy expectation value. See Appendix B for more detailed explanation.

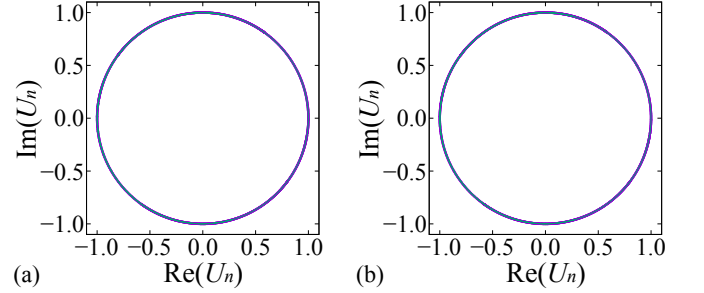


FIG. 3: The eigenvalues of the time-evolution operator, which is the product of the operators in Eqs. (1), (2) and (3), for (a) $g=0$ and (b) $g=1$ (purple markers) on the unit circle (green line) in the complex plane.

B. Non-Hermiticity and laser pumping

We can understand the physical meaning of the factor g in the non-Hermitian Hamiltonian in Eqs. (4) in terms of the rate equations for a two-level system as discussed in Refs. [61, 62].

Let us consider $N_1 + N_2$ pieces of two-level systems under external laser pumping with the occupation number of atoms N_1 and N_2 in the ground and excited states, respectively; the total number of atoms is fixed to $N = N_1 + N_2$. In the case with no stimulated emission, we obtain the rate equations for the occupation number of the two states as follows:

$$\frac{dN_1}{dt} = w_{12}N_2 - w_{21}N_1 + (N_2 - N_1)Wn, \quad (10)$$

$$\frac{dN_2}{dt} = w_{21}N_1 - w_{12}N_2 - (N_2 - N_1)Wn. \quad (11)$$

Here, w_{21} is the transition rate of the photons from the ground state to the excited state due to external pumping and w_{12} is the decay rate from the excited state to the ground state due to

spontaneous emission. We let n denote the number of photons in the environment and W is the transition rate of decay to the environment. We can make a correspondence between the two rates and the elements of the Hamiltonian H_{NH} in Eq. (4), using Fermi's golden rule as follows [63]:

$$w_{21} = |\langle E | H_{\text{NH}} | G \rangle|^2 = w^2 e^{2g}, \quad (12)$$

$$w_{12} = |\langle G | H_{\text{NH}} | E \rangle|^2 = w^2 e^{-2g}. \quad (13)$$

Subtracting Eq. (11) from Eq. (10) yields

$$\frac{dD}{dt} = (w_{21} - w_{12})N - (w_{21} + w_{12})D - 2WnD \quad (14)$$

with

$$N := N_1 + N_2 = \text{const.}, \quad D := N_2 - N_1. \quad (15)$$

In the stationary state for which the left-hand side of the equation above vanishes, we have

$$D = \frac{w_{21} - w_{12}}{w_{21} + w_{12} + 2Wn_0} N \quad (16)$$

with fixed number of photons in the environment n_0 ; the whole system is pumped by laser and n stays in the same value. From Eqs. (15) and (16), the ratio between the occupation numbers of the two states in the stationary state is given by

$$\begin{aligned} \frac{N_2^{\text{st}}}{N_1^{\text{st}}} &= \frac{N + D}{N - D} = \frac{w_{21} + Wn_0}{w_{12} + Wn_0} = \frac{w^2 e^{2g} + Wn_0}{w^2 e^{-2g} + Wn_0} \\ &\simeq \frac{w^2 e^{2g}}{Wn_0} \propto e^{2g} \end{aligned} \quad (17)$$

for the stationary values N_1^{st} and N_2^{st} for N_1 and N_2 , respectively. We used the relation $w^2 e^{-2g} \ll Wn_0 \ll w^2 e^{2g}$ with g being a finite value. We can thus regard that the parameter g describes the probability difference between the two levels of a qubit under laser pumping. Since this parameter g does not depend on the other parameter ε in Eqs. (1) and (29), these two parameters are set mutually independently.

C. Numerical results for the one-dimensional model

We here present our results of numerical calculation in one dimension. Starting with computation on a flat line, we first examine basic properties of our model. Then we will show results for the topological edge states in Sec. II C 2 and for an effective harmonic potential in Sec. II C 3. We set $\hbar = a = 1$ here in Sec. II C for all numerical calculations for the one-dimensional model and in Sec. III B for those for the two-dimensional model.

We define the normalized probability distribution as in

$$\tilde{P}(x, T) := \frac{P(x, T)}{\sum_x P(x, T)}, \quad (18)$$

where

$$P(x, T) := |\langle x | \psi^{\text{R}}(T) \rangle|^2. \quad (19)$$

We note the fact that $\sum_x P(x, T)$ is not conserved for a finite value of g . Refer to Appendix B for the definitions of $|\psi^{\text{R}}\rangle$ and $\langle \psi^{\text{R}} | := |\psi^{\text{R}}\rangle^\dagger$. We also define the mean position $\langle x(T) \rangle$ and the standard deviation $\Delta x(T)$ of the walker at each time step as in

$$\langle x(T) \rangle := \sum_x x \tilde{P}(x, T), \quad (20)$$

$$\Delta x(T) := \sqrt{\sum_x [(x - \langle x(T) \rangle)^2 \tilde{P}(x, T)]}, \quad (21)$$

respectively.

1. Dynamics on a flat potential

We first look at dynamics of our quantum active particle without any potentials, namely, on a flat line. Let us set the parameters for the coin operator (2), θ_{G} and θ_{E} , to the following constants:

$$\theta_{\text{G/E}}(x) = \theta_{\text{g/e}} := \theta_0 \pm \varepsilon. \quad (22)$$

As explained below Eq. (5), we choose this parametrization so that $\theta_{\text{e}} < \theta_{\text{g}}$. All the computation described throughout Sec. II C 1 was conducted with parameter values fixed as follows unless noted with other parameter values:

$$\theta_0 = \frac{\pi}{3}, \quad \varepsilon = 0.25, \quad w = 0.25, \quad (23)$$

and the system size is $L_x = 401$ with $-200 \leq x \leq 200$.

Figure 4 shows the normalized probability distributions $\tilde{P}(x, T)$ after 100 time steps of evolution from the initial condition of the delta peak only in the ground state at the origin site. The time evolution of the ground state shown in Fig. 4(a) is a typical probability distribution of quantum walks. In quantum walks, all possible paths leading to the origin site should interfere with each other and be cancelled out, which yields the minimum around the origin. Meanwhile, the paths leading to the wave fronts on the left and the right should be less in number and be cancelled less, which yields the maximum peaks around the wave fronts.

On the other hand, the normalized probability distribution of the time evolution in the excited state shown in Fig. 4(b) exhibits a more complicated structure. The peaks on the outside (indicated by the arrows) are due to the fact that our quantum active particle runs faster in the excited state than in the ground state. The peaks on the inside are due to the transition from the peaks of the ground state, which runs more slowly than in the excited state. When we further turn on the non-Hermitian activity parameter g , the probability for the excited state is pumped up from the one in Fig. 4 (b) to the higher one in Fig. 4 (d). This clearly demonstrates the dynamics that we explain in Fig. 2.

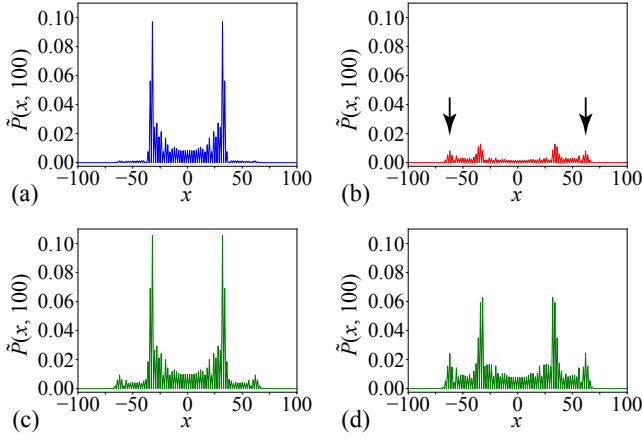


FIG. 4: Normalized probability distributions $\tilde{P}(x, T = 100)$ of ground state [(a)], excited state [(b)] and the sum of both states [(c), (d)] after 100 time steps of evolution for $g = 0$ [(a), (b), (c)] and $g = 1$ [(d)]. The system size is $L_x = 401$ with $-200 \leq x \leq 200$; the probability outside the plotting range is significantly small.

Let us quantitatively discuss how fast our quantum walker runs. In Fig. 4 (a) and (b), the peak locations for the ground state are ± 32 after 100 time steps and those for the excited state are ± 62 . If there were no coupling between the ground and excited states, the front peaks of each state run in the group velocity $\cos \theta_{g/e}$ [64]; see Appendix C. In the particular case of the parameter values in Eq. (22) with Eq. (23), we would have

$$\cos \theta_g \simeq 0.270, \quad \cos \theta_e \simeq 0.698. \quad (24)$$

When we introduce a coupling between the ground and excited states, however, we numerically found for the parameter values $\varepsilon = w = 0.25$ (see also Appendix C) that the maximum group velocity for the ground state is about 0.343 at $k \simeq 0.624\pi$ and the one for the excited states is about 0.642 at $k \simeq 0.450\pi$. This is consistent with the numerical observations (0.32 and 0.62 , respectively) in Fig. 4 (a) and (b). This indicates that the faster running peaks of the excited state are dragged down by the more slowly running peaks of the ground states, while the latter are pulled up by the former.

As is discussed in Sec. II B, we can understand that our quantum active particle, which has two levels, is pumped from the lower level to a higher one by an external laser. Hence there exists an oscillation between the ground and excited states. Figure 5 shows the time dependence of the standard deviation calculated for different parameter values. First, Fig. 5 (a) shows the case in which there is no coupling between the ground and excited states: $w = 0$. In this case, the standard deviations of both the ground and excited states as well as their sum converge to one curve; since there is no transition between the two states, we do not observe an oscillation.

When we turn on w into finite values as in Fig. 5 (b)–(d), we observe that the standard deviations of both the ground and excited states oscillate with a relative phase shift π , which implies the resonant transition between two states. This reso-

nant transition is one of the quantum features that we observe in our quantum active matter. For detailed discussion on the time period of the oscillations T_{osc} , see Appendix D. Notice that the standard deviation normalized by the total probability, which is plotted with green plus marks, do not oscillate in the case of $g = 0$ (Fig. 5 (b)) but it does in the case of $g > 0$ (Fig. 5 (c), (d)). This is because as we increase g , the ratio of the excited state increases as e^{2g} and physical quantities such as the means and the standard deviations of the total system tend to take closer values to those of the excited state. The oscillations that we will see in Fig. 11 (c), (d) and Fig. 15 (b) below can be explained in the same way.

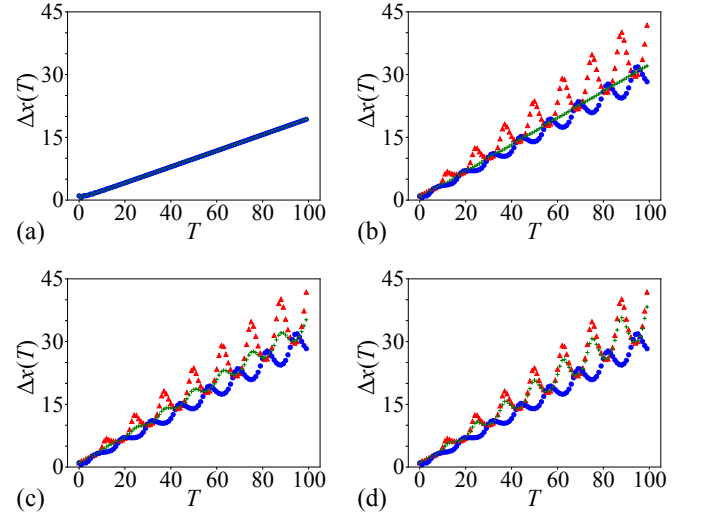


FIG. 5: The time-step dependence of the standard deviation Δx for $w = 0$ [(a)] and $w = 0.25$ [(b), (c), (d)]. (a) and (b) are computed for $g = 0$, (c) is computed for $g = 0.5$, and (d) is computed for $g = 1$. Red triangles and blue circles indicate the standard deviation with respect to the excited and ground states, respectively. Green plus marks indicate the standard deviation normalized by the total probability.

2. Topological edge states

Next we study edge states of our quantum active particle. We here set the parameters for the coin operator (2), θ_G and θ_E , as

$$\theta_{G/E}(x) = \begin{cases} \theta_{g/e} & \text{for } x \leq 0 \\ -\theta_{g/e} & \text{for } x > 0 \end{cases}, \quad \theta_{g/e} := \theta_0 \pm \varepsilon. \quad (25)$$

so that edge states may emerge at the discontinuities of the parameter values at the origin $x = 0$ and at the edges of the system $x = \pm L/2$, where L denotes the system size and we assume the periodic boundary condition. The appearance of these states bound to the edges was predicted in Refs. [57, 65] for the Dirac Hamiltonian in one dimension; note that the quantum walk converges to the Dirac system in the continuum

limit [2, 57]. Since the potential of Eq. (25) squared is a constant potential, the states other than the edge states propagate as those in Sec. II C 1.

We first set the initial state to the edge state at $x = 0$ of the ground state under the condition of no transition between the ground and excited states. We then let the state evolve in time with the transition w turned on. We thereby expect

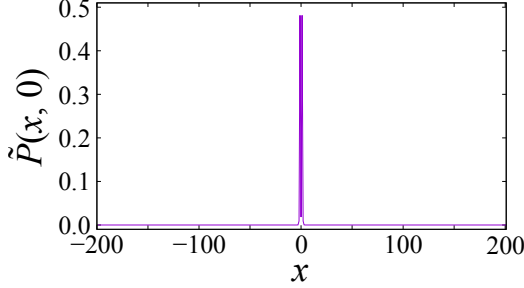


FIG. 6: The edge state of the ground state localized around $x = 0$, which we used as the initial state for the time evolution shown in Fig. 7.

that the edge state of the ground state may remain bounded to the edge, whereas the component pumped up to the excited state may escape away from the edge. The time evolution in Fig. 7 precisely reproduces our expectation. All the computation described throughout Sec. II C 2 was conducted with the parameter values fixed as follows:

$$\theta_0 = \frac{\pi}{3}, \quad \varepsilon = 0.25, \quad w = 0.25. \quad (26)$$

In Fig. 7(c), most of the wave function of the ground state stays around the origin $x = 0$, whereas some of the component pumped up to the excited state runs away from the edge as shown in Fig. 7(e). Note that a small fraction of the ground state that leaks away in Fig. 7(c) is in fact the component that transits back down from the excited-state component escaping to the outside, then running behind the excited state.

As we turn on the activity parameter g , the significant fraction of the excited state escapes away from the bound of the edge as exhibited in Fig. 7(f). This indeed demonstrates the fact that the quantum walker is activated by the parameter g .

3. One-dimensional oscillator

We finally investigate dynamics of our quantum active particle under an effective harmonic potential. For the purpose, we set the parameters for the coin operator (2), θ_G and θ_E , linear in x :

$$\theta_{G/E}(x) = \begin{cases} \theta_{g/e} & \text{for } x < \frac{-\alpha-1}{\beta} \\ \theta_{g/e}(\alpha + \beta x) & \text{for } \frac{-\alpha-1}{\beta} \leq x \leq \frac{-\alpha+1}{\beta} \\ -\theta_{g/e} & \text{for } x > \frac{-\alpha+1}{\beta} \end{cases}, \quad (27)$$

$$\theta_{g/e} := \theta_0 \pm \varepsilon.$$

While the Dirac particle in the continuum limit of the quantum walk [2] perceives the linear potential in Eq. (27), the

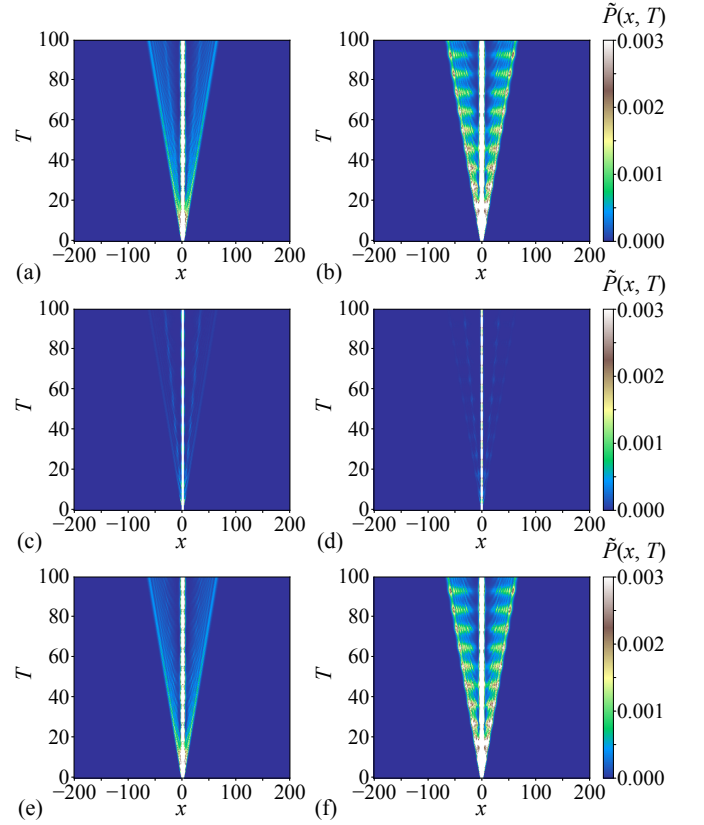


FIG. 7: The density plot of the time evolution of the quantum walker focusing on the ground state [(c), (d)], the excited state [(e), (f)] and the sum of the two states [(a), (b)] for $g = 0$ [(a), (c), (e)] and $g = 1$ [(b), (d), (f)]. The color indicates the probability of the walker at each site and time step.

corresponding Schrödinger particle perceives [57] the potential squared, which is a harmonic potential in the region $(-\alpha - 1)/\beta \leq x \leq (-\alpha + 1)/\beta$. All the computation described throughout Sec. II C 3 was conducted with parameters fixed as follows:

$$\theta_0 = \frac{\pi}{8}, \quad \varepsilon = 0.25, \quad w = 0.25, \quad \alpha = 1, \quad \beta = 0.025. \quad (28)$$

We show in Fig. 8 the potential of Eq. (27) squared, which the corresponding Schrödinger particle in the continuum limit (cf. Ref. [57]) perceives.

For the initial state for the computation, we shift to the right by δ_x sites an eigenstate of the eigenvalue close to unity with the parameters in Eq. (28) and $g = 0$, which we numerically found; see Fig. 9.

We first investigate the dependence of the survival probability in the potential, in the region of $-80 \leq x \leq 0$, on δ_x and g ; see Fig. 10. (Here the system size is $L_x = 401$ with $-200 \leq x \leq 200$ under the periodic boundary conditions.) Starting from $g = 0$, we see that the survival probability decreases as g increases to some point, but at around $g = 2$ (depending on δ_x , which is the number of steps we shift the

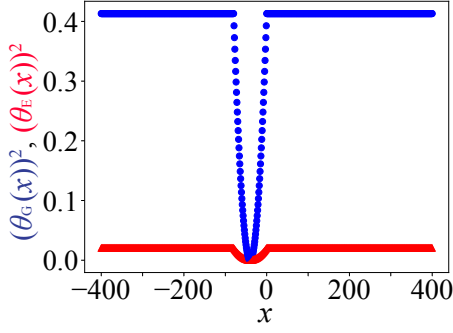


FIG. 8: Potential of Eq. (27) squared with the parameters in Eq. (28) and $L_x = 801$. The vertical axis indicates the squared potentials for the ground state (blue markers) and the excited state (red markers). The horizontal axis indicates the space.

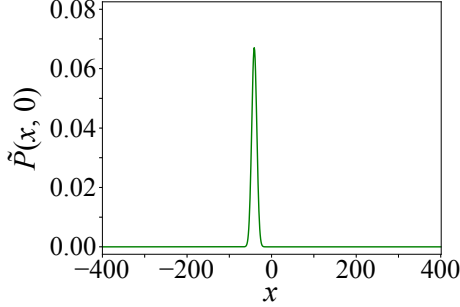


FIG. 9: An eigenstate of the eigenvalue close to unity, $U_n = 0.9378050525983931 + i0.3471623299278579$, with the parameters in Eq. (28) and $L_x = 801$, $g = 0$, which we numerically found with a FORTRAN program. The eigenstate is shifted $\delta_x = 19$ steps to the right to be made into the initial state for the computation of dynamics.

eigenstate), it starts slightly increasing and converges to a constant up to $g = 10$, for which the probability almost comes from the excited state.

We then look into the dynamics of our quantum active particle more closely for larger system size, $L_x = 801$ with $-400 \leq x \leq 400$ under the periodic boundary conditions. For the initial state for the computation hereafter, we fix the shift to $\delta_x = 19$ sites. The mean position $\langle x(T) \rangle$ and the standard deviation $\Delta x(T)$ of the walker at each time step are shown in Fig. 11. The fluctuations in Fig. 11(c), (d) for $g = 1$ come from the non-conservation of probability. We notice in Fig. 11(b), (d) that the standard deviation tends to take larger values as g increases. The difference for different values of g comes not just from the change of the ratio between the ground and excited states; in Fig. 11, we see the difference in each of the two states.

The normalized probability distribution of the ground and the excited states at each site after 400 time steps of evolution are shown in the left column of Fig. 12. We can see that the side peaks indicated by the arrows become relatively larger compared to the peak around the center as g increases. With

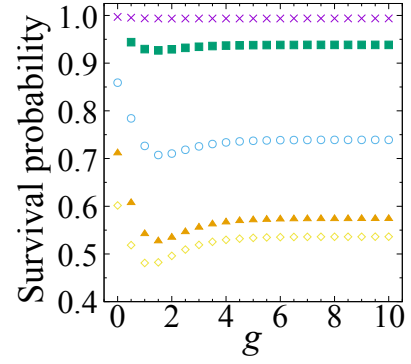


FIG. 10: The dependence of the survival probability in the potential, in the region of $-80 \leq x \leq 0$, on δ_x and g . We plot the survival probability for $\delta_x = 9, 14, 19, 24$ and 29 with purple crosses, green-filled squares, blue circles, orange-filled triangles and yellow diamonds, respectively.

this, we claim that we succeeded in defining a quantum active particle using non-unitary quantum walks; we obtained similar results as in the previous research [1] on a classical active Brownian particle, that is, the particle becomes more active and climbs up the potential. Note that our non-Hermiticity parameter g corresponds to the energy-take-up term $q(\mathbf{r})$ in the previous research [1].

Meanwhile, we also observed unique quantum features. The right column of Fig. 12 shows density plots of the time evolution. We can clearly see the ballistic spreading of the side peaks of the excited state, particularly for $g = 1$. We see that some curves first emerge on the $x > 0$ region. This is because we shift the eigenstate of the time-evolution operator to x plus direction to make it into the initial state. Our quantum active particle hits the potential wall on the right side which is located at $-40 \leq x \leq 0$ first and then some portion climbs up the wall and escape outside around $T \simeq 10$. Some portion is reflected on the right potential wall and then hits the potential on the left side which is located at $-80 \leq x \leq -40$. Then likewise some portion climbs up the potential wall and escape outside around $T \simeq 100$, and some portion is reflected. Our quantum active particle repeats the same; more peaks are separated from the central peak around $T \simeq 200$ and $T \simeq 300$ too.

III. QUANTUM ACTIVE PARTICLE IN TWO DIMENSIONS

A. Two-dimensional model

We define quantum active matter in two dimensions, “non-unitarizing” the discrete-time quantum walk in two dimensions, which was very recently proposed in Ref. [57]. Our quantum active walker now has eight internal states in total, namely, $(|L\rangle \oplus |R\rangle) \otimes (|D\rangle \oplus |U\rangle) \otimes (|G\rangle \oplus |E\rangle) = |LDG\rangle \oplus |RDG\rangle \oplus |LUG\rangle \oplus |RUG\rangle \oplus |LDE\rangle \oplus |RDE\rangle \oplus |LUE\rangle \oplus |RUE\rangle$. Here, $|U\rangle$, $|D\rangle$, $|R\rangle$ and $|L\rangle$ denote up-

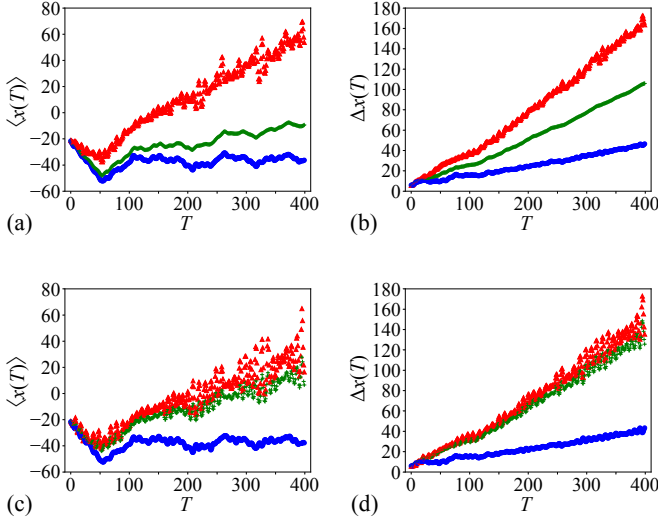


FIG. 11: The mean position [(a), (c)] and the standard deviation [(b), (d)] of the movement of the quantum walker for $g = 0$ [(a), (b)] and $g = 1$ [(c), (d)]. The vertical axis indicates the mean position and the standard deviation, while the horizontal axis indicates the time steps. Red triangles and blue circles indicate the mean and the standard deviation with respect to the excited and ground states, respectively. Green plus marks indicate the mean position and the standard deviation normalized by the total probability.

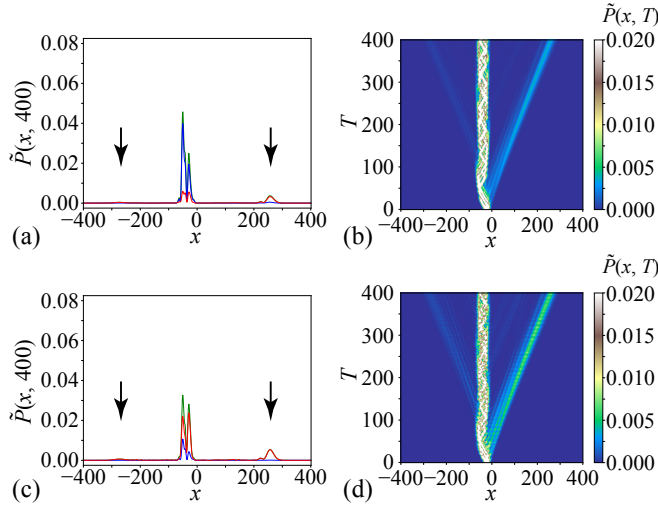


FIG. 12: The normalized probability distribution $\tilde{P}(x, T = 400)$. [(a), (c)] and the density plot of the time evolution [(b), (d)] of the quantum walker for $g = 0$ [(a), (b)] and $g = 1$ [(c), (d)]. For (a) and (c), red curves and blue curves correspond to the excited and ground states, respectively, while green curves indicate the sum of the probabilities for both states. For (b) and (d), the vertical axis indicates the time steps and the horizontal axis indicates the site. The color indicates the probability of the walker at each site and time step.

ward, downward, rightward and leftward states, respectively, while $|G\rangle$ and $|E\rangle$ denote the ground and excited states, respectively. We fix the ordering of the basis vectors in this way in the present Sec. III A. We define the time evolution of our two-dimensional quantum active particle $|\psi(T)\rangle = [U^{(2)}(g)]^T |\psi(0)\rangle$ for $T \in \mathbb{Z}$ in terms of the following operators:

$$N^{(2)}(g) := \sum_{x,y} [|x, y\rangle\langle x, y| \otimes e^{-iH_{\text{NH}}^{(2)}(g)}], \quad (29)$$

$$C_x^{(2)} := \bigotimes_{x,y} e^{-i\theta_{x,G}(x)(\sigma^y \otimes \tau^0 \otimes v^G) - i\theta_{x,E}(x)(\sigma^y \otimes \tau^0 \otimes v^E)} \quad (30)$$

$$= \sum_{x,y} [|x, y\rangle\langle x, y| \otimes C_x^{(2)}(x)], \quad (31)$$

$$S_x^{(2)} := e^{-a(\sigma^z \otimes \tau^0 \otimes v^0) \partial_x} \quad (32)$$

$$= \sum_{x,y} [|x, y\rangle\langle x, y| \otimes S_x^{(2)}(x)], \quad (33)$$

$$C_y^{(2)} := \bigotimes_{x,y} e^{-i\theta_{y,G}(y)(\sigma^x \otimes \tau^y \otimes v^G) - i\theta_{y,E}(y)(\sigma^x \otimes \tau^y \otimes v^E)} \quad (34)$$

$$= \sum_{x,y} [|x, y\rangle\langle x, y| \otimes C_y^{(2)}(y)], \quad (35)$$

$$S_y^{(2)} := e^{-a(\sigma^x \otimes \tau^z \otimes v^0) \partial_y} \quad (36)$$

$$= \sum_{x,y} [|x, y\rangle\langle x, y| \otimes S_y^{(2)}(y)], \quad (37)$$

with $U^{(2)}(g) := S_y^{(2)} C_y^{(2)} S_x^{(2)} C_x^{(2)} N^{(2)}(g)$. Here,

$$H_{\text{NH}}^{(2)}(g) := \sigma^0 \otimes \tau^0 \otimes \begin{pmatrix} -\varepsilon & -we^{-g} \\ -we^{+g} & +\varepsilon \end{pmatrix}. \quad (38)$$

The operators $C_x^{(2)}(x)$, $S_x^{(2)}(x)$, $C_y^{(2)}(y)$ and $S_y^{(2)}(y)$ read

$$\begin{aligned} C_x^{(2)}(x) &= \begin{pmatrix} +c_{x,G}(x) & -s_{x,G}(x) \\ +s_{x,G}(x) & +c_{x,G}(x) \end{pmatrix} \otimes v^G \\ &+ \begin{pmatrix} +c_{x,E}(x) & -s_{x,E}(x) \\ +s_{x,E}(x) & +c_{x,E}(x) \end{pmatrix} \otimes v^E, \end{aligned} \quad (39)$$

$$S_x^{(2)}(x) = \begin{pmatrix} P_x & & & \\ & Q_x & & \\ & & P_x & \\ & & & Q_x \end{pmatrix} \otimes v^0, \quad (40)$$

$$\begin{aligned} C_y^{(2)}(y) &= \begin{pmatrix} +c_{y,G}(y) & & -s_{y,G}(y) \\ & +c_{y,G}(y) & -s_{y,G}(y) \\ & +s_{y,G}(y) & +c_{y,G}(y) \\ +s_{y,G}(y) & & & +c_{y,G}(y) \end{pmatrix} \otimes v^G \end{aligned}$$

$$+ \begin{pmatrix} +c_{y,E}(y) & & -s_{y,E}(y) \\ & +c_{y,E}(y) & -s_{y,E}(y) \\ & +s_{y,E}(y) & +c_{y,E}(y) \\ +s_{y,E}(y) & & +c_{y,E}(y) \end{pmatrix} \otimes v^E, \quad (41)$$

$$S_y^{(2)}(y) = \begin{pmatrix} P_y & Q_y \\ Q_y & P_y \\ & P_y & -Q_y \\ -Q_y & & P_y \end{pmatrix} \otimes v^0, \quad (42)$$

where

$$\begin{aligned} c_{x,G}(x) &:= \cos(\theta_{x,G}(x)), & s_{x,G}(x) &:= \sin(\theta_{x,G}(x)), \\ c_{x,E}(x) &:= \cos(\theta_{x,E}(x)), & s_{x,E}(x) &:= \sin(\theta_{x,E}(x)), \\ c_{y,G}(y) &:= \cos(\theta_{y,G}(y)), & s_{y,G}(y) &:= \sin(\theta_{y,G}(y)), \\ c_{y,E}(y) &:= \cos(\theta_{y,E}(y)), & s_{y,E}(y) &:= \sin(\theta_{y,E}(y)), \\ P_x &:= |x-a, y\rangle\langle x, y|, & Q_x &:= |x+a, y\rangle\langle x, y|, \\ P_y &:= \frac{1}{2}(|x, y-a\rangle\langle x, y| + |x, y+a\rangle\langle x, y|), \\ Q_y &:= \frac{1}{2}(|x, y-a\rangle\langle x, y| - |x, y+a\rangle\langle x, y|). \end{aligned} \quad (43)$$

We let $\{\sigma^x, \sigma^y, \sigma^z\}$, $\{\tau^x, \tau^y, \tau^z\}$ and $\{v^x, v^y, v^z\}$ denote the Pauli matrices for the spaces spanned by $\{|L\rangle, |R\rangle\}$, $\{|D\rangle, |U\rangle\}$ and $\{|G\rangle, |E\rangle\}$, respectively. The identity matrix for each space is given by σ^0 , τ^0 and v^0 , respectively, and $v^{G/E} := (1 \pm v^z)/2$. Note that $S_x^{(2)}$ and $S_y^{(2)}$ are identical to the ones in Eq. (17) in Ref. [57] except for the factor v^0 , while $C_x^{(2)}$ and $C_y^{(2)}$ are extensions of the ones in Eq. (17) in Ref. [57] with the factors v^G and v^E .

B. Numerical results for the two-dimensional model

For numerical calculation in two dimensions, we set the system size to $L_x = L_y = 71$ with $-35 \leq x \leq 35$ and $-35 \leq y \leq 35$. We again introduce linear potentials as phases of the coin operators:

$$\theta_{x,G/E}(x) = \begin{cases} \theta_{g/e} & \text{for } x < \frac{-\alpha-1}{\beta} \\ \theta_{g/e}(\alpha + \beta x) & \text{for } \frac{-\alpha-1}{\beta} \leq x \leq \frac{-\alpha+1}{\beta} \\ -\theta_{g/e} & \text{for } x > \frac{-\alpha+1}{\beta} \end{cases}, \quad (44)$$

$$\theta_{x,G/E}(y) = \begin{cases} \theta_{g/e} & \text{for } y < \frac{-\alpha-1}{\beta} \\ \theta_{g/e}(\alpha + \beta y) & \text{for } \frac{-\alpha-1}{\beta} \leq y \leq \frac{-\alpha+1}{\beta} \\ -\theta_{g/e} & \text{for } y > \frac{-\alpha+1}{\beta} \end{cases}, \quad (45)$$

$$\theta_{g/e} = \theta_0 \pm \varepsilon. \quad (46)$$

The potential of Eqs. (44) and (45) squared is a harmonic potential [57] with its top cut off.

All the computation described throughout this section was conducted with the parameters fixed as follows:

$$\theta_0 = \frac{\pi}{8}, \quad \varepsilon = 0.25, \quad w = 0.25, \quad \alpha = 0.5, \quad \beta = 0.05. \quad (47)$$

For the initial state, we used an eigenstate of the eigenvalue close to unity (Fig. 13) shift to x by nine sites and imposed the initial velocity in the form of $e^{i(k_x x + k_y y)}$ with $(k_x, k_y) = (0, \pi)$.

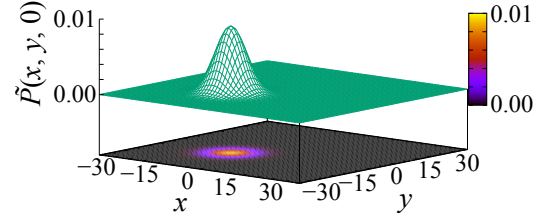


FIG. 13: An eigenstate for the eigenvalue close to unity, $U_n = 0.9336010518344118 + i0.3583142140826795$, with the parameters in Eq. (44) and $g = 0$, which was computed with a FORTRAN program. The eigenstate is shifted $(\delta_x, \delta_y) = (9, 0)$ steps and is induced initial velocity in the form of $e^{i(k_x x + k_y y)}$ with $(k_x, k_y) = (0, \pi)$ to be made into the initial state for the computation of dynamics.

Figure 14 shows the expectation values,

$$\langle x(T) \rangle := \sum_{x,y} x \tilde{P}(x, y, T), \quad (48)$$

$$\langle y(T) \rangle := \sum_{x,y} y \tilde{P}(x, y, T) \quad (49)$$

at each time step, where

$$P(x, y, T) := |\langle x, y | \psi^R(T) \rangle|^2, \quad (50)$$

$$\tilde{P}(x, y, T) := \frac{P(x, y, T)}{\sum_{x,y} P(x, y, T)}. \quad (51)$$

We observe that our quantum active particle moves around in wider region with larger values of g . This is a result similar to the previous research [1] in a classical system; see also Fig. 16. Meanwhile, we observe in Fig. 14(a) that the movement of our quantum active particle almost converges to a limit cycle for $g = 0$, not falling into the origin. This is a quantum feature: our quantum active particle stays on the constant energy surface.

The standard deviations $\Delta x(T)$ and $\Delta y(T)$ of the walker at each time step

$$\Delta x(T) := \sqrt{\sum_{x,y} [(x - \langle x(T) \rangle)^2 \tilde{P}(x, y, T)]}, \quad (52)$$

$$\Delta y(T) := \sqrt{\sum_{x,y} [(y - \langle y(T) \rangle)^2 \tilde{P}(x, y, T)]} \quad (53)$$

are shown in Fig. 15. We can clearly see that the standard deviation tends to take larger values as g increases. This means that our quantum active walker moves around more actively when it takes up more energy from the environment. This is also a result similar to the previous research [1] in a classical system. Meanwhile, we again observe oscillation in Fig. 15 as

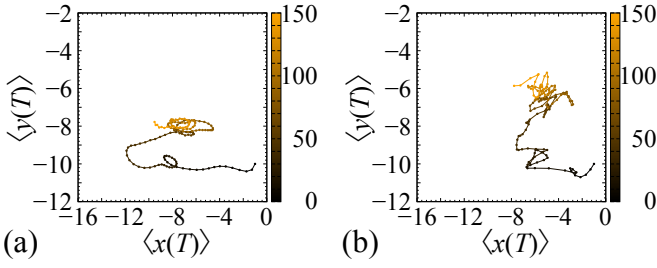


FIG. 14: The orbit of the quantum walker for (a) $g = 0$ and (b) $g = 1$. The vertical axis indicates $\langle y(T) \rangle$ and the horizontal axis indicates $\langle x(T) \rangle$. Black circles indicate the values at the beginning of time evolution and they turn into orange as time goes on.

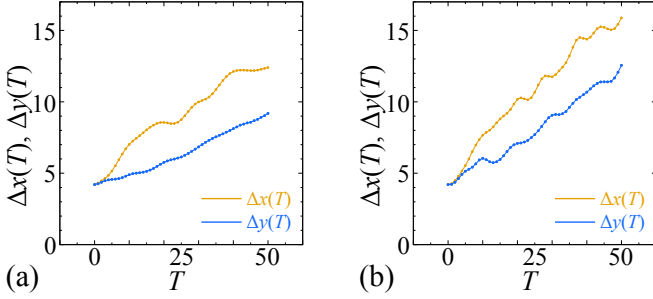


FIG. 15: The time-step dependence of the standard deviations Δx (yellow lines) and Δy (blue lines) for (a) $g = 0$ and (b) $g = 1$. We only plot standard deviations during $0 \leq T \leq 50$ since standard deviations outside the plotting range are not reliable due to the periodic boundary condition; wave functions reach the edge by around $T \simeq 50$ as you can see in Fig. 16.

in Fig. 5. This resonant transition between two states is again one of the quantum features that we observe.

The normalized probability distribution of the sum of the ground and the excited states at each site after 40 time steps are shown in Fig. 16. We can see that the side peaks become relatively larger compared to the peak around the center as g increases.

IV. SUMMARY

In the present paper, motivated by a study [1] on an active Brownian particle, we newly introduced a model of quantum active matter by “non-unitarizing” the quantum walk in one and two dimensions. Our quantum active matter allows us to study real-time dynamics of the system in a fully quantum range without external manipulation [23]. This kind of quantum active matter was first realized in our model. Taking into account the two properties of quantum active matter,

- (i) neither energy nor momentum are conserved;
- (ii) the kinetic motion depends on particles’ internal states,

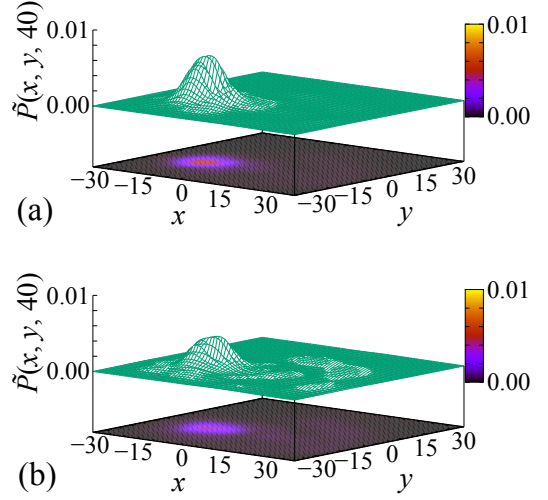


FIG. 16: The normalized probability distribution of the quantum walker $\tilde{P}(x, y, 40)$ after 40 time steps of time evolution for (a) $g = 0$ and (b) $g = 1$.

we expect that our research will open up new research avenues in two ways as in Table I.

In order to realize dynamics under a harmonic potential in a two-dimensional system, we used the newly proposed unitary discrete-time quantum walk [57], whose dynamics is similar to that of a Schrödinger particle under a harmonic potential in two dimensions. We introduced a new internal degree of freedom, namely, the energy ground state $|G\rangle$ and excited state $|E\rangle$, to realize a quantum system without energy nor momentum conservation. With these new internal states, we also introduced a new non-unitary operator $N(g)$ for an asymmetric transition between $|G\rangle$ and $|E\rangle$, which realizes an open quantum system without energy conservation. The non-Hermiticity parameter g promotes transition to the excited state, which represents the situation that the particle takes up energy from the environment. We realized a system without momentum conservation by manipulating the parameter θ for the coin operator for a discrete-time quantum walk; we utilized the property that the continuum limit of a one-dimensional discrete-time quantum walk gives the Dirac equation with its mass proportional to the parameter θ . We have studied with our model similarities to the previous research on a classical system [1] but also observed unique quantum phenomena as follows:

1. Similarities to classical active particle: The movement of the quantum walker becomes more active in a non-trivial way as we increase the non-Hermiticity parameter g ; looking at the excited state and the ground state only, we can still recognize difference of dynamics with different values of g .
2. Unique quantum features: Oscillations emerge due to the resonant transition between the ground and excited states in one and two dimensions, peak propagates ballistically in one dimension, and the quantum walker stays on the constant energy surface in two dimensions.

For future prospect, it may be interesting to study topological properties of our quantum active matter model and compare them to those of Ref. [57]. Furthermore, we are interested in how our quantum active particle behaves if we relax the pseudo-Hermiticity condition (8) and make the energy eigenvalues complex, which means that the probability density increases or decreases exponentially. As another direction, introducing decoherence may make the present quantum system converges to an active Brownian system. We lastly discuss experimental realization of our model. Quantum walks themselves are already realized in various systems: *e.g.* cold atom systems [66], laser systems [67] and photon systems [47, 68, 69]. Focusing especially on laser systems, we can realize the ground and excited states by utilizing optical device with different transmittance. By coupling two systems with each of the ground state and the excited state, we may be able to realize our quantum active particle in experiments.

ACKNOWLEDGEMENT

We are grateful for Ryo Hanai, Ken-Ichiro Imura, Yuta Kuroda, Franco Nori, Kazuki Sone, Kazuaki Takasan and Kazumasa A. Takeuchi for fruitful discussions. The computation in this work has been done partly using the facilities of the Supercomputer Center, the Institute for Solid State Physics, the University of Tokyo. This work is supported by JSPS KAKENHI Grant Numbers JP19H00658, JP20H01828, JP21H01005 and JP22H01140. This work was supported by RIKEN Junior Research Associate Program.

Appendix A: Review of quantum walks in one dimension and higher dimensions

1. One-dimensional quantum walks

The quantum walk was first proposed in one dimension [26]. In addition to the spatial degree of freedom $|x\rangle$, we let each lattice point have an internal degree of freedom of two states $|L\rangle$ and $|R\rangle$. The entire state space is thereby spanned by $|x\rangle \otimes |L\rangle$ and $|x\rangle \otimes |R\rangle$.

The shift operator \tilde{S} is defined to move the spatial part of the state according to the internal degree of freedom:

$$\tilde{S} := \sum_x [|x-a\rangle\langle x| \otimes |L\rangle\langle L| + |x+a\rangle\langle x| \otimes |R\rangle\langle R|], \quad (\text{A1})$$

where a is the lattice constant. In other words, the wave function of the component $|L\rangle$ is shifted to the left by one lattice constant, while that of $|R\rangle$ is shifted to the right by one lattice constant. (Note that throughout the paper, we put the lattice constant a to unity, for simplicity.) If we kept operating the shift operator only, the left-going component would keep moving left, while the right-going component would keep moving right, without any interaction between them. We hence additionally introduce the coin operator

$$\tilde{C} := \sum_x [|x\rangle\langle x| \otimes u], \quad (\text{A2})$$

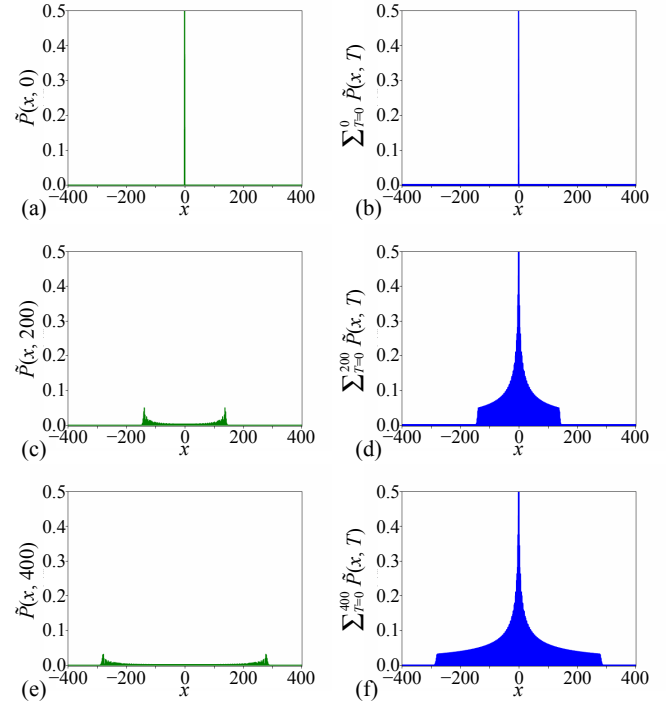


FIG. 17: A numerical example of the probability distribution [(a), (c), (e)] and the temporal sum of the probability [(b), (d), (f)] of the quantum walker after 0 [(a), (b)], 200 [(c), (d)] and 400 [(e), (f)] time steps of evolution in one dimension under the initial condition (A4).

where u is a 2×2 unitary matrix that shuffles the left-going and right-going components at each lattice point. Throughout the present paper we use the following specific form for the unitary u :

$$u = \begin{pmatrix} \cos \theta & -\sin \theta \\ \sin \theta & \cos \theta \end{pmatrix}. \quad (\text{A3})$$

Taking the initial state

$$|\psi(0)\rangle = \frac{1}{\sqrt{2}} |0\rangle \otimes (|L\rangle + i|R\rangle), \quad (\text{A4})$$

for example, and applying the shift and coin operators repeatedly as in

$$|\psi(T)\rangle = (\tilde{S}\tilde{C})^T |\psi(0)\rangle, \quad (\text{A5})$$

we observe the probability distribution $\langle \psi(T) | \psi(T) \rangle$ in Fig. 17(a).

We can understand this probability distribution as follows. In classical random walks, the walker that starts from the origin takes various paths stochastically. Each path has its own positive probability. Since there are more paths around the starting point, the probability accumulates higher around there. In quantum walks, on the other hand, each path has its own amplitude, which is generally complex. Although there

are more paths around the starting point, they interfere with each other because of their random phases instead of the probability accumulation. This interference decreases the probability around the origin. Since the number of paths is small near the right and left wave fronts, the interference is weaker, and hence the probability has peaks there.

2. Two-dimensional quantum walks

A consistent definition of two-dimensional quantum walks was introduced in Ref. [57]. It starts with the identification of the one-dimensional Dirac Hamiltonian

$$H_D^{(1)} = cp_x\sigma^z + m_x\sigma^y \quad (\text{A6})$$

as an approximate generator of the one-dimensional quantum walk [2], where p_x is the momentum operator in the x direction, m_x is a mass term, and σ^z and σ^y are the Pauli matrices that represent the inner degree of freedom of the Dirac particle. The Trotter decomposition of dynamics due to the Dirac Hamiltonian (A6) yields the dynamics (A5), where the light speed c is proportional to the lattice constant and m_x is proportional to θ in Eq. (A3).

In squaring the Dirac Hamiltonian (A6), we note that the crossing term disappear because the Pauli matrices are elements of the two-dimensional Clifford algebra: $\sigma^z\sigma^y + \sigma^y\sigma^z = 0$. This motivates us to introduce [57] the Dirac Hamiltonian in two spatial dimensions in the form

$$H_D^{(2)} = (cp_x\sigma^z + m_x\sigma^y) \otimes \tau^0 + \sigma^z \otimes (cp_y\tau^z + m_y\tau^y), \quad (\text{A7})$$

where p_y is the momentum operator in the y direction, m_y is an additional mass term, and τ^z and τ^y are the Pauli matrices in an additional inner degree of freedom with τ^0 being the 2×2 identity matrix in the additional space. In squaring the newly introduced Dirac Hamiltonian (A7) in two spatial dimensions, we note that all crossing terms disappear because the four operators $\sigma^z \otimes \tau^0$, $\sigma^y \otimes \tau^0$, $\sigma^x \otimes \tau^z$ and $\sigma^x \otimes \tau^y$ are elements of the four-dimensional Clifford algebra. The Trotter decomposition of the dynamics due to the Dirac Hamiltonian (A7) yields a consistent definition of quantum walk in two spatial dimensions [57]. It is now straightforward to extend the quantum walk to three and higher-dimensional ones.

Appendix B: Lack of orthonormality in non-Hermitian Hamiltonians

We here show that in spite of the fact that the pseudo-energy eigenvalues are all fixed to real values, because of the lack of orthonormality of the eigenvectors, the probability and the energy expectation value generally oscillate in time, as we stress at the end of Sec. II A.

Let us consider a general non-Hermitian Hamiltonian H with $H^\dagger \neq H$. Its eigenvectors are defined in the following

manner:

$$\begin{cases} H|\psi_n^R\rangle = E_n|\psi_n^R\rangle & \text{for a right-eigenvector } |\psi_n^R\rangle, \\ \langle\psi_n^L|H = \langle\psi_n^L|E_n & \text{for a left-eigenvector } \langle\psi_n^L|. \end{cases} \quad (\text{B1})$$

Note that the latter is often represented in the form

$$H^\dagger|\psi_n^L\rangle = E_n^*|\psi_n^L\rangle, \quad (\text{B2})$$

where $|\psi_n^L\rangle := \langle\psi_n^L|^\dagger$. In other words, the right- and left-eigenvectors of a non-Hermitian matrix H are essentially the right-eigenvectors of H and H^\dagger , respectively. With the definition (B1), the eigenvectors satisfy bi-orthonormality

$$\langle\psi_n^L|\psi_m^R\rangle = \delta_{nm} \quad (\text{B3})$$

under proper normalization, but the orthonormality is not in general satisfied:

$$\langle\psi_n^R|\psi_m^R\rangle \neq \delta_{nm}, \quad (\text{B4})$$

where $\langle\psi_n^R| := |\psi_n^R\rangle^\dagger$.

Let us specifically look at our non-Hermitian Hamiltonian $H_{\text{NH}}(g)$ (1) as an example. As shown in Eqs. (7) and (8), we can make the non-Hermitian matrix $H_{\text{NH}}(g)$ Hermitian with the imaginary gauge transformation (7) [58, 59] with an imaginary vector potential g . Let $|\psi_n\rangle$ denote the eigenvector for the Hermitian Hamiltonian $H_{\text{NH}}(g=0)$:

$$H_{\text{NH}}(g=0)|\psi_n\rangle = E_n|\psi_n\rangle, \quad (\text{B5})$$

$$\langle\psi_n|H_{\text{NH}}(g=0) = \langle\psi_n|E_n. \quad (\text{B6})$$

Note that in this case of the Hermitian Hamiltonian $H_{\text{NH}}(g=0)$, the left-eigenvector $\langle\psi_n|$ and the Hermitian conjugate of the right-eigenvector $|\psi_n\rangle$ are the same as in $|\psi_n\rangle = \langle\psi_n|^\dagger$ and the eigenvectors satisfy the standard orthonormality

$$\langle\psi_n|\psi_m\rangle = \delta_{nm}. \quad (\text{B7})$$

From Eqs. (7) and (B5), we obtain the following:

$$A(g)^{-1}H_{\text{NH}}(g)A(g)|\psi_n\rangle = E_n|\psi_n\rangle. \quad (\text{B8})$$

Operating $A(g)$ from the left on each side of Eq. (B8) yields

$$H_{\text{NH}}(g)[A(g)|\psi_n\rangle] = E_n[A(g)|\psi_n\rangle]. \quad (\text{B9})$$

We thereby notice that if we take $|\psi_n^R\rangle$ as in

$$|\psi_n^R\rangle = A(g)|\psi_n\rangle, \quad (\text{B10})$$

then Eq. (B9) is in the completely same form as the top line of Eq. (B1). Similarly, from Eqs. (7) and (B6), we obtain

$$[\langle\psi_n|A(g)^{-1}]H_{\text{NH}}(g) = [\langle\psi_n|A(g)^{-1}]E_n. \quad (\text{B11})$$

Thus we take $\langle\psi_n^L|$ as in

$$\langle\psi_n^L| = \langle\psi_n|A(g)^{-1} \quad (\text{B12})$$

to obtain the bottom line of Eq. (B1). From Eqs. (B7), (B10) and (B12), we can easily check that the bi-orthonormality (B3) is satisfied while the orthonormality (B4) is not unless $A(g)^\dagger A(g) = \mathbb{I}$, which holds only for $g = 0$ in our case of the non-Hermitian Hamiltonian $H_{\text{NH}}(g)$.

Let us next consider the time evolution of eigenvectors of a general non-Hermitian Hamiltonian H . We assume that the Schrödinger equation for a non-Hermitian Hamiltonian H has the forms

$$\begin{cases} i \frac{d}{dt} |\psi^{\text{R}}(t)\rangle = H |\psi^{\text{R}}(t)\rangle, \\ -i \frac{d}{dt} \langle \psi^{\text{L}}(t)| = \langle \psi^{\text{L}}(t)| H, \end{cases} \quad (\text{B13})$$

where we put \hbar to unity. The latter equation may look more plausible in the form

$$i \frac{d}{dt} |\psi^{\text{L}}(t)\rangle = H^\dagger |\psi^{\text{L}}(t)\rangle. \quad (\text{B14})$$

In other words, the right- and left-eigenvectors are driven by the non-Hermitian Hamiltonians H and H^\dagger , respectively. This, combined with Eq. (B1), results in the time-evolution of the forms

$$\begin{cases} |\psi_n^{\text{R}}(T)\rangle = e^{-iE_n T} |\psi_n^{\text{R}}(0)\rangle, \\ \langle \psi_n^{\text{L}}(T)| = e^{+iE_n T} \langle \psi_n^{\text{L}}(0)|, \end{cases} \quad (\text{B15})$$

which keeps the bi-orthonormality (B3) intact for any T . Thus if we calculate the probability density with the left- and right-eigenvectors, it does not depend on time:

$$\begin{aligned} \langle \psi^{\text{L}}(T) | \psi^{\text{R}}(T) \rangle &= \sum_{n,m} c_m^* c_n e^{i(E_m - E_n)T} \langle \psi_m^{\text{L}} | \psi_n^{\text{R}} \rangle \\ &= \sum_n |c_n|^2, \end{aligned} \quad (\text{B16})$$

where we expanded the initial states as

$$\begin{cases} |\psi^{\text{R}}(0)\rangle = \sum_n c_n |\psi_n^{\text{R}}\rangle, \\ \langle \psi^{\text{L}}(0)| = \sum_m c_m^* \langle \psi_m^{\text{L}}|. \end{cases} \quad (\text{B17})$$

The energy expectation value defined in the form $\langle \psi^{\text{L}}(T) | H | \psi^{\text{R}}(T) \rangle$ is conserved because

$$\begin{aligned} \langle \psi^{\text{L}}(T) | H | \psi^{\text{R}}(T) \rangle &= \sum_{n,m} c_m^* c_n e^{i(E_m - E_n)T} \langle \psi_m^{\text{L}} | H | \psi_n^{\text{R}} \rangle \\ &= \sum_n |c_n|^2 E_n. \end{aligned} \quad (\text{B18})$$

On the other hand, if we calculate the probability density with the right-eigenvectors and their Hermitian conjugate, then it fluctuates depending on time as follows:

$$\langle \psi^{\text{R}}(T) | \psi^{\text{R}}(T) \rangle = \sum_{n,m} c_m^* c_n e^{i(E_m^* - E_n)T} \langle \psi_m^{\text{R}} | \psi_n^{\text{R}} \rangle, \quad (\text{B19})$$

whose last factor is not reduced to δ_{mn} because of the inequality (B4). Note that since the imaginary gauge transformation $A(g)$ in Eq. (7) for our model is Hermitian, we have $A(g)^\dagger A(g) = A(g)^2 \neq \mathbb{I}$, and hence specifically

$$\langle \psi_m^{\text{R}} | \psi_n^{\text{R}} \rangle = \langle \psi_m | A(g)^2 | \psi_n \rangle \neq \delta_{mn} \quad (\text{B20})$$

unless $g = 0$. Similarly, we can check that the energy expectation value defined in the form $\langle \psi^{\text{R}}(T) | H | \psi^{\text{R}}(T) \rangle$ is not conserved because

$$\begin{aligned} \langle \psi^{\text{R}}(T) | H | \psi^{\text{R}}(T) \rangle &= \sum_{n,m} c_m^* c_n e^{i(E_m^* - E_n)T} \langle \psi_m^{\text{R}} | H | \psi_n^{\text{R}} \rangle \\ &= \sum_{n,m} c_m^* c_n e^{i(E_m^* - E_n)T} E_n \langle \psi_m^{\text{R}} | \psi_n^{\text{R}} \rangle. \end{aligned} \quad (\text{B21})$$

The reason why we use in the present paper the right-eigenvectors and their Hermitian conjugate is because our model is an open quantum system. There are two ways of understanding non-Hermitian systems; one is the closed non-Hermitian system and the other is the open quantum system [70, 71]. The original concept of the PT -symmetric non-Hermitian system [72, 73] was to replace the Hermiticity with more physical symmetries in making certain that the expectation values of the energy and other physical observables are real. Since the system is considered to be closed in this framework, we should employ the right- and left-eigenvectors to keep the bi-orthogonality (B3) satisfied and to make the energy expectation value constant in time as in Eq. (B18).

The open quantum system, on the other hand, is considered to be embedded in an environment and the entire system of the central system combined with the environment is supposedly Hermitian. Therefore, we should employ the standard way of calculating the expectation value of an observable, if it is localized in the central system or not, by employing the right-eigenvectors and their Hermitian conjugate as in Eq. (B21). Since the open quantum system can exchange the probability and the energy with the environment, it is natural that the probability density and the energy expectation value are not constant in time.

Appendix C: Peak velocity of the quantum walkers

We here present the derivation of the peak velocity of quantum walkers, which we used in the discussions around Eq. (24). Consider first the case without the operator $N(g)$, for which the walkers in the ground and excited states are independent of each other. We can then derive the peak velocity as follows. For brevity, let us drop the suffices G and E for the moment and put $\hbar = a = 1$, so that x is an integer.

The walker in each state evolves in time according to the following shift and coin operators:

$$\tilde{S} := \sum_x \left[|x-1\rangle\langle x| \otimes \begin{pmatrix} 1 & 0 \\ 0 & 0 \end{pmatrix} + |x+1\rangle\langle x| \otimes \begin{pmatrix} 0 & 0 \\ 0 & 1 \end{pmatrix} \right], \quad (\text{C1})$$

$$\tilde{C} := \sum_x \left[|x\rangle\langle x| \otimes \begin{pmatrix} \cos \theta & -\sin \theta \\ \sin \theta & \cos \theta \end{pmatrix} \right], \quad (\text{C2})$$

where we represent the inner degree of freedom of two states $|L\rangle$ and $|R\rangle$ in Eqs. (A1)–(A3) in terms of 2×2 matrices and we put the lattice constant a to unity. In order to analyze the dynamics efficiently, let us introduce the Fourier transformation in the following forms:

$$|x\rangle = \frac{1}{\sqrt{2\pi}} \int_{-\pi}^{\pi} e^{-ikx} |k\rangle dk, \quad (\text{C3})$$

$$|k\rangle = \frac{1}{\sqrt{2\pi}} \sum_{x=-\infty}^{\infty} e^{ikx} |x\rangle. \quad (\text{C4})$$

It casts the shift and coin operators into the forms

$$\tilde{S} = \int_{-\pi}^{\pi} dk |k\rangle\langle k| \otimes \begin{pmatrix} e^{ik} & 0 \\ 0 & e^{-ik} \end{pmatrix}, \quad (\text{C5})$$

$$\tilde{C} = \int_{-\pi}^{\pi} dk |k\rangle\langle k| \otimes \begin{pmatrix} \cos \theta & -\sin \theta \\ \sin \theta & \cos \theta \end{pmatrix}. \quad (\text{C6})$$

We are now in a position to analyze each subspace of k separately. The two eigenvalues of

$$\begin{pmatrix} e^{ik} & 0 \\ 0 & e^{-ik} \end{pmatrix} \begin{pmatrix} \cos \theta & -\sin \theta \\ \sin \theta & \cos \theta \end{pmatrix} \quad (\text{C7})$$

are given in the form of

$$\lambda_{\pm}(k) := \cos k \cos \theta \pm i\sqrt{1 - \cos^2 k \cos^2 \theta} \quad (\text{C8})$$

or

$$\lambda_{\pm}(k) = e^{\pm iE(k)} \quad (\text{C9})$$

with the relation [64]

$$\cos E(k) = \cos k \cos \theta. \quad (\text{C10})$$

The last relation gives the dispersion relation of the quantum walk. The group velocity is then given by

$$v_g(k) := \frac{dE}{dk} = \frac{\sin k}{\sin E(k)} \cos \theta. \quad (\text{C11})$$

Its maximum with respect to k should give the peak velocity of the quantum walk because the peaks are the front runners. By further differentiating Eq. (C11), we have

$$\begin{aligned} \frac{dv_g}{dk} &= \left(\frac{\cos k}{\sin E} - \frac{\sin k \cos E \times v_g}{\sin^2 E} \right) \cos \theta \\ &= \frac{\cos k}{\sin^3 E} \sin^2 \theta \cos \theta. \end{aligned} \quad (\text{C12})$$

This thereby shows that the component of $k = \pi/2$ runs fastest and its group velocity gives the peak velocity of the free random walker. Since Eq. (C10) produces $\cos E(k) = 0$ and $\sin E(k) = \pm 1$ at $k = \pi/2$, the peak velocity of the free random walker is $v_g(\pi/2) = \cos \theta$. We used this fact in Eq. (24).

When we have a finite operator $N(g)$, which connects the ground and excited states, we should move over to the 4×4 matrices, again in the Fourier space:

$$C_k := \begin{pmatrix} \cos \theta_g & -\sin \theta_g & & \\ \sin \theta_g & \cos \theta_g & & \\ & & \cos \theta_e & -\sin \theta_e \\ & & \sin \theta_e & \cos \theta_e \end{pmatrix} \quad (\text{C13})$$

$$S_k := \begin{pmatrix} e^{ik} & & & \\ & e^{-ik} & & \\ & & e^{ik} & \\ & & & e^{-ik} \end{pmatrix} \quad (\text{C14})$$

$$\begin{aligned} N_k(g) &:= \exp \left[-i \begin{pmatrix} -\epsilon & & -we^{-g} & \\ & -\epsilon & & -we^{-g} \\ -we^{+g} & & \epsilon & \\ & -we^{+g} & & \epsilon \end{pmatrix} \right] \\ &= \begin{pmatrix} \xi - i\epsilon\eta & & iwe^{-g}\eta & \\ iwe^{+g}\eta & \xi - i\epsilon\eta & & iwe^{-g}\eta \\ & iwe^{+g}\eta & \xi + i\epsilon\eta & \\ & & & \xi + i\epsilon\eta \end{pmatrix}, \end{aligned} \quad (\text{C15})$$

where

$$\xi := \cos \sqrt{\epsilon^2 + w^2}, \quad \eta := \frac{\sin \sqrt{\epsilon^2 + w^2}}{\sqrt{\epsilon^2 + w^2}}. \quad (\text{C16})$$

We thereby numerically find the four eigenvalues of $i \ln S_k C_k N_k(g)$ in the case of Eq. (23) as in Fig. 18(a) and compute the group velocity according to each eigenvalue as in Fig. 18(b). For $\epsilon = w = 0$, the red and green curves as well as the orange and blue curves in Fig. 18 would be degenerate. Introduction of finite values of w and ϵ lift the degeneracy; now the green and blue curves are for the ground state, while the red and orange curves are for the excited states. We can indeed observe that the corresponding group velocity for the excited state is greater than the one for the ground state for all k except for $k = 0$ and $k = \pi$. This numerically confirms the expectation that the quantum walker runs faster in the excited state than in the ground state.

For the specific parameter values of Eq. (23), the maximum of each group velocity gives about ± 0.343 at $k \simeq 0.624\pi$ and ± 0.642 at $k \simeq 0.450\pi$ as indicated by arrows in the figure, which we quoted below Eq. (24).

Appendix D: Probability oscillations between the ground and excited states

Here we explain that our active quantum walk is approximately described by an effective two-level Hamiltonian. The description is consistent with the oscillations found in Fig. 5.

We notice in Fig. 18(a), or equivalently in Fig. 19(c) that the upper two levels are the closest to each other at $k = 0$, and symmetrically, the lower two levels at $k = \pi$. We thereby approximately derive an effective Hamiltonian for each set of two levels and show that resonant oscillations between the two levels at the minimum energy gap is quantitatively consistent with the oscillation that we find in Fig. 5. We also show an

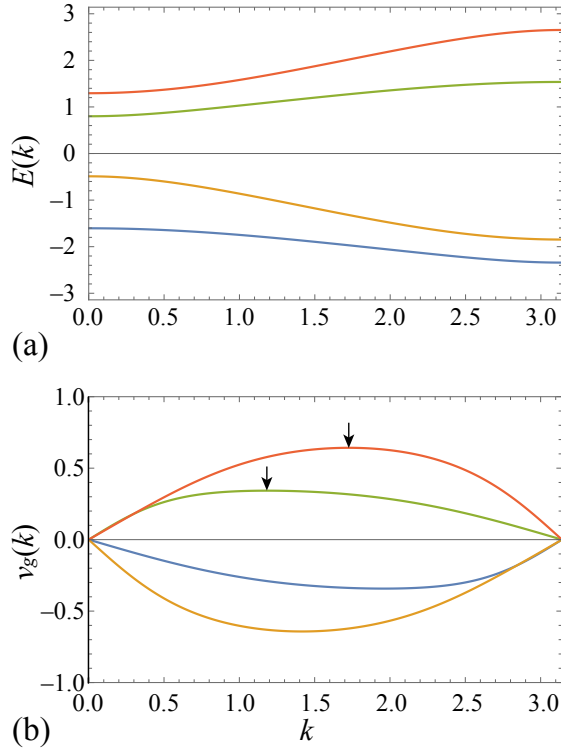


FIG. 18: (a) The k -dependence of the four energy eigenvalues; in other words, the dispersion relation. (b) The k -dependence of the group velocity. The arrows indicate the maxima of the group velocities for the first and second largest eigenvalues. The parameter values are the ones specified in Eq. (23). We do not show the values for $-\pi < k < 0$ because the dispersion relation is symmetric with respect to $k = 0$ and the group velocity is π -periodic.

amplification of the probability in the excited level by the factor of e^{2g} , which is also consistent with Eq. (17).

As shown in Fig. 19(a), the ground and excited states are degenerate for $\varepsilon = w = 0$, for which the upper and lower blocks of C_k in Eq. (C13) are equal to each other and $N_k(g)$ in Eq. (C15) is reduced to the identity operator. When we turn on ε to 0.25 but keep $w = 0$ as in Fig. 19(b), the degeneracy between the ground and excited states are lifted except for $k = 0$ for the upper levels and $k = \pi$ for the lower levels. When we further turn on w to 0.25 as in Fig. 19(c), the degeneracies at $k = 0$ and $k = \pi$ are both lifted. We claim that this smallest energy gaps cause the oscillations found in Fig. 5.

Let us here focus on the energy gap at $k = 0$ between the upper two levels, and estimate it by perturbation theory up to the first order of w , keeping ε finite. For $k = 0$, the shift operator (C14) is reduced to the identity operator, and hence irrelevant. The coin operator (C14) keeps the same form. For the operator (C15), the unperturbed limit yields

$$N_g^{(0)} = \begin{pmatrix} e^{i\varepsilon} & & & \\ & e^{i\varepsilon} & & \\ & & e^{-i\varepsilon} & \\ & & & e^{-i\varepsilon} \end{pmatrix}, \quad (\text{D1})$$

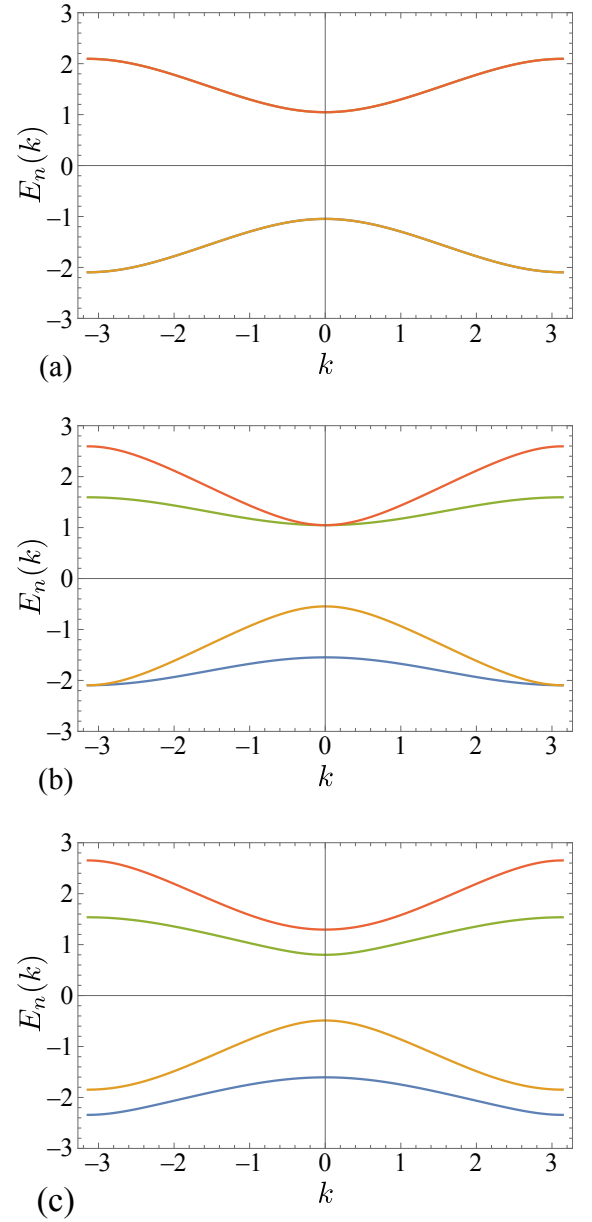


FIG. 19: The dispersion relation of the four pseudo-energy eigenvalues for (a) $\varepsilon = w = 0$, (b) $\varepsilon = 0.25$ with $w = 0$, and (c) $\varepsilon = w = 0.25$. In Panel (a), two curves are degenerate in each of the two curves. Panel (c) is equivalent to Fig. 18(a) but in a doubled plotting region. In all cases, we set $\theta_0 = \pi/3$.

whereas the first-order perturbation is given by

$$N_g^{(1)} = iw\eta_0 \begin{pmatrix} & e^{-g} & & \\ e^{+g} & & e^{-g} & \\ & e^{+g} & & \end{pmatrix} \quad (\text{D2})$$

with $\eta_0 = \sin(\varepsilon)/\varepsilon$. The perturbation parameter w in ξ and η of Eq. (C16) only contributes to the second-order perturbation, which we neglect hereafter. (Do not confuse the super-

scripts $^{(0)}$ and $^{(1)}$, which denote in the present Appendix the order of the perturbation, with the same superscripts in the main text, which there denote the dimensionality of the quantum walk.)

To summarize, the unperturbed time-evolution operator for $k = 0$ is

$$U_0^{(0)} := C_0 N_g^{(0)} = \begin{pmatrix} e^{i\varepsilon} \begin{pmatrix} \cos \theta_g & -\sin \theta_g \\ \sin \theta_g & \cos \theta_g \end{pmatrix} & \\ & e^{-i\varepsilon} \begin{pmatrix} \cos \theta_e & -\sin \theta_e \\ \sin \theta_e & \cos \theta_e \end{pmatrix} \end{pmatrix} \quad (\text{D3})$$

$$= \begin{pmatrix} e^{-i(\theta_g \sigma_y - \varepsilon)} & \\ & e^{-i(\theta_e \sigma_y + \varepsilon)} \end{pmatrix}, \quad (\text{D4})$$

while the first-order perturbation is given by

$$U_0^{(1)} := C_0 N_g^{(1)} = iw\eta_0 \begin{pmatrix} & e^{-g} \begin{pmatrix} \cos \theta_g & -\sin \theta_g \\ \sin \theta_g & \cos \theta_g \end{pmatrix} \\ e^{+g} \begin{pmatrix} \cos \theta_e & -\sin \theta_e \\ \sin \theta_e & \cos \theta_e \end{pmatrix} & \end{pmatrix}. \quad (\text{D5})$$

The unperturbed eigenvectors that diagonalize the unperturbed matrix (D4) are

$$|\psi_{g+}^{(0)}\rangle = \frac{1}{\sqrt{2}} \begin{pmatrix} 1 \\ i \\ 0 \end{pmatrix}, \quad |\psi_{e+}^{(0)}\rangle = \frac{1}{\sqrt{2}} \begin{pmatrix} 0 \\ 0 \\ 1 \\ i \end{pmatrix}, \quad (\text{D6})$$

$$|\psi_{g-}^{(0)}\rangle = \frac{1}{\sqrt{2}} \begin{pmatrix} 1 \\ -i \\ 0 \\ 0 \end{pmatrix}, \quad |\psi_{e-}^{(0)}\rangle = \frac{1}{\sqrt{2}} \begin{pmatrix} 0 \\ 0 \\ 1 \\ -i \end{pmatrix}, \quad (\text{D7})$$

which give the unperturbed eigenvalues as

$$\lambda_{g+}^{(0)} = e^{-i(\theta_g - \varepsilon)} = e^{-i\theta_0}, \quad \lambda_{e+}^{(0)} = e^{-i(\theta_e + \varepsilon)} = e^{-i\theta_0}, \quad (\text{D8})$$

$$\lambda_{g-}^{(0)} = e^{-i(-\theta_g - \varepsilon)}, \quad \lambda_{e-}^{(0)} = e^{-i(-\theta_e + \varepsilon)}. \quad (\text{D9})$$

The eigenvalues $\lambda_{g+}^{(0)}$ and $\lambda_{e+}^{(0)}$ in Eq. (D8) correspond to the positive pseudo-energies, which are degenerate to θ_0 as in the upper two levels of Fig. 19(b). (The eigenvalues $\lambda_{g-}^{(0)}$ and $\lambda_{e-}^{(0)}$ are degenerate to the negative pseudo-energy $-\theta_0$ at $k = \pi$ rather than $k = 0$.)

In other words, the unperturbed eigenvectors in Eq. (D6) both give the same eigenvalue $e^{-i\theta_0}$. We therefore diagonalized the following matrix to find the first-order perturbed eigenvalues:

$$\Delta U = \begin{pmatrix} \langle \psi_{g+}^{(0)} | U_0^{(1)} | \psi_{g+}^{(0)} \rangle & \langle \psi_{g+}^{(0)} | U_0^{(1)} | \psi_{e+}^{(0)} \rangle \\ \langle \psi_{e+}^{(0)} | U_0^{(1)} | \psi_{g+}^{(0)} \rangle & \langle \psi_{e+}^{(0)} | U_0^{(1)} | \psi_{e+}^{(0)} \rangle \end{pmatrix}. \quad (\text{D10})$$

Straightforward algebra produces

$$\Delta U = iw\eta_0 e^{-i\theta_0} \begin{pmatrix} 0 & e^{-g-i\varepsilon} \\ e^{+g+i\varepsilon} & 0 \end{pmatrix}. \quad (\text{D11})$$

Since the eigenvalues of the matrix above are ± 1 , we have the eigenvalues up to the first order of w in the form

$$\lambda_{\pm} \simeq e^{-i\theta_0} (1 \pm iw\eta_0). \quad (\text{D12})$$

The pseudo-energy eigenvalues are thereby given by

$$E_{\pm} := i \log \lambda_{\pm} \simeq \theta_0 \mp w\eta_0. \quad (\text{D13})$$

Therefore, the energy gap at $k = 0$ is found to be $\Delta E = 2w\eta_0$. For $\varepsilon = 0.25$ and $w = 0.25$, we have $\Delta E \simeq 0.494808$. The period of the oscillation is $2\pi/\Delta E \simeq 12.6982$, which is consistent with the oscillation found in Fig. 5.

Let us finally find the effective Hamiltonian that governs the dynamics in the Hilbert subspace of the two vectors in Eq. (D6). The matrix

$$V := \begin{pmatrix} 1 & e^{-g-i\varepsilon} \\ e^{+g+i\varepsilon} & -1 \end{pmatrix} \quad (\text{D14})$$

diagonalizes ΔU with

$$V^{-1} = \frac{1}{-2} \begin{pmatrix} -1 & -e^{-g-i\varepsilon} \\ -e^{+g+i\varepsilon} & 1 \end{pmatrix} = \frac{V}{2} \quad (\text{D15})$$

as in $V^{-1}\Delta UV = \text{diag}(\lambda_+, \lambda_-)$. This implies that the effective Hamiltonian is given by

$$H_{\text{eff}} := V \begin{pmatrix} E_+ & \\ & E_- \end{pmatrix} V^{-1} \quad (\text{D16})$$

$$= \begin{pmatrix} \theta_0 & -w\eta_0 e^{-g-i\varepsilon} \\ -w\eta_0 e^{+g+i\varepsilon} & \theta_0 \end{pmatrix}. \quad (\text{D17})$$

The effective time-evolution operator within this Hilbert subspace is therefore found to be

$$U_{\text{eff}}^T := e^{-iH_{\text{eff}}T} = e^{-i\theta_0 T} \exp \left[iw\eta_0 T \begin{pmatrix} 0 & e^{-g-i\varepsilon} \\ e^{+g+i\varepsilon} & 0 \end{pmatrix} \right] \quad (\text{D18})$$

In calculating the matrix exponential above, we take full advantage of the complex gauge transformation described in Eqs. (7) and (8). Using the gauge transformation

$$A(g+i\varepsilon) = \begin{pmatrix} e^{-(g+i\varepsilon)/2} & 0 \\ 0 & e^{+(g+i\varepsilon)/2} \end{pmatrix}, \quad (\text{D19})$$

we have

$$A^{-1} \begin{pmatrix} 0 & e^{-g-i\varepsilon} \\ e^{+g+i\varepsilon} & 0 \end{pmatrix} A = \begin{pmatrix} 0 & 1 \\ 1 & 0 \end{pmatrix}. \quad (\text{D20})$$

We therefore find

$$\exp \left[iw\eta_0 T \begin{pmatrix} 0 & e^{-g-i\varepsilon} \\ e^{+g+i\varepsilon} & 0 \end{pmatrix} \right] \quad (\text{D21})$$

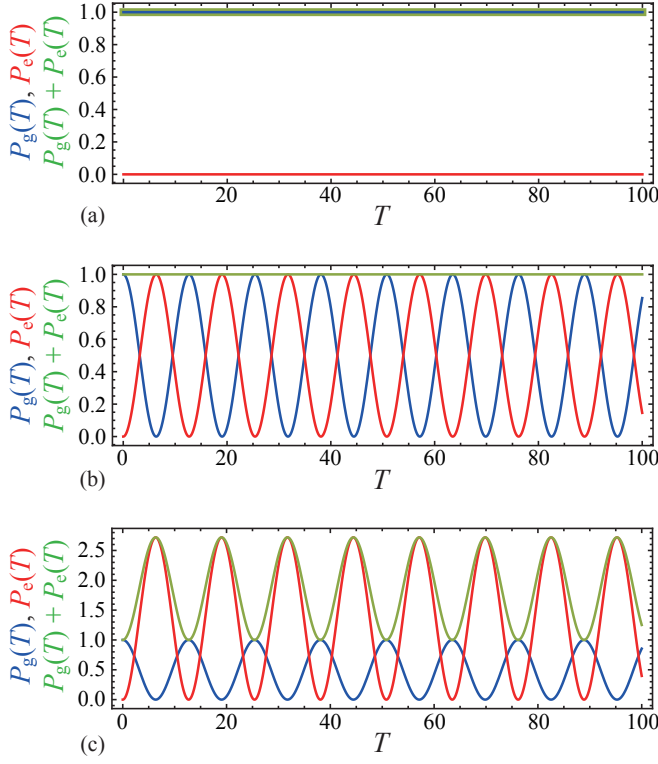


FIG. 20: The oscillation of the probabilities in Eqs. (D25) and (D26). In each panel, the horizontal axis indicates t , the blue curve indicates $P_g(t)$, the red curve indicates $P_e(t)$, and the green curve indicates the summation. (a) $w = 0$ and $g = 0$. (b) $w = 0.25$ and $g = 0$. (c) $w = 0.25$ and $g = 0.5$.

$$= A \begin{pmatrix} \cos(w\eta_0 T) & i \sin(w\eta_0 T) \\ i \sin(w\eta_0 T) & \cos(w\eta_0 T) \end{pmatrix} A^{-1} \quad (\text{D22})$$

$$= \begin{pmatrix} \cos(w\eta_0 T) & i e^{-g-i\varepsilon} \sin(w\eta_0 T) \\ i e^{+g+i\varepsilon} \sin(w\eta_0 T) & \cos(w\eta_0 T) \end{pmatrix} \quad (\text{D23})$$

Suppose, for example, that we start the time evolution from

$|\psi_{g+}^{(0)}\rangle$. We thereby find

$$|\psi_{+}(T)\rangle := U_{\text{eff}}^T |\psi_{g+}^{(0)}\rangle = e^{-i\theta_0 T} \begin{pmatrix} \cos(w\eta_0 T) \\ i e^{+g+i\varepsilon} \sin(w\eta_0 T) \end{pmatrix} \quad (\text{D24})$$

Therefore the following probabilities for the ground and excited states oscillate as in

$$P_g(T) := \left| \langle \psi_{g+}^{(0)} | U_{\text{eff}}^T | \psi_{g+}^{(0)} \rangle \right|^2 = \cos^2(w\eta_0 T), \quad (\text{D25})$$

$$P_e(T) := \left| \langle \psi_{e+}^{(0)} | U_{\text{eff}}^T | \psi_{g+}^{(0)} \rangle \right|^2 = e^{2g} \sin^2(w\eta_0 T); \quad (\text{D26})$$

see Fig. 20. For $g = 0$, this simply describes the resonant oscillation between the ground and excited states with the probability conservation $P_g(T) + P_e(T) = 1$. For $g > 0$, we find the enhancement of the oscillation amplitude of the excited state by the factor of e^{2g} , which is consistent with Eq. (17). The oscillation should describe the behavior that we observe in Fig. 5.

For $w = 0$ as in Fig. 20(a), the ground and excited states of the effective Hamiltonian are degenerate and we do not observe any difference or oscillation between the two states. This corresponds to the case of Fig. 5(a). As we introduce the off-diagonal elements of N_g to be $w = 0.25$, the oscillation of the phase difference of π for the ground and excited states appears with the period $\pi/(w\eta_0) \simeq 12.6982$ for $\varepsilon = 0.25$, or about 8 oscillations in the range $0 \leq T \leq 100$, which is consistent with what we observe in Fig. 5(b). We notice nonetheless that the value for the sum of the two states (green line) constantly increases without any oscillations in Fig. 5(b). This corresponds to the probability conservation $P_g(T) + P_e(T) = 1$. Finally, when we introduce g as in Fig. 5(c) and (d), we see that the green curve now oscillates with the same phase as the value for the excited state. This implies that the oscillation amplitude of the excited state is enhanced by the factor e^{2g} , which is consistent with the observation in Eq. (D26).

- [1] Frank Schweitzer, Werner Ebeling, and Benno Tilch. Complex Motion of Brownian Particles with Energy Depots. *Phys. Rev. Lett.*, 80:5044–5047, Jun 1998.
- [2] Frederick W. Strauch. Relativistic quantum walks. *Phys. Rev. A*, 73:054302, May 2006.
- [3] Len Pismen. *Active matter within and around us*. Frontiers Collection. Springer Nature, Cham, Switzerland, 1 edition, February 2021.
- [4] P Romanczuk, M Bär, W Ebeling, B Lindner, and L Schimansky-Geier. Active Brownian particles. *The European Physical Journal Special Topics*, 202(1):1–162, March 2012.
- [5] Gabriel Popkin. The physics of life. *Nature*, 529(7584):16–18, 2016.
- [6] Daniel Needleman and Zvonimir Dogic. Active matter at the interface between materials science and cell biology. *Nature Reviews Materials*, 2(9):17048, 2017.
- [7] Amin Doostmohammadi, Jordi Ignés-Mullol, Julia M. Yeomans, and Francesc Sagués. Active nematics. *Nature Communications*, 9(1):3246, 2018.

- [8] Gerhard Gompper, Roland G Winkler, Thomas Speck, Alexandre Solon, Cesare Nardini, Fernando Peruani, Hartmut Löwen, Ramin Golestanian, U Benjamin Kaupp, Luis Alvarez, Thomas Kiørboe, Eric Lauga, Wilson C K Poon, Antonio DeSimone, Santiago Mui nos Landin, Alexander Fischer, Nicola A Söker, Frank Cichos, Raymond Kapral, Pierre Gaspard, Marisol Ripoll, Francesc Sagues, Amin Doostmohammadi, Julia M Yeomans, Igor S Aranson, Clemens Bechinger, Holger Stark, Charlotte K Hemelrijk, François J Nedelec, Trinish Sarkar, Thibault Aryaksama, Mathilde Lacroix, Guillaume Duclos, Victor Yashunsky, Pascal Silberzan, Marino Arroyo, and Sohan Kale. The 2020 motile active matter roadmap. *Journal of Physics: Condensed Matter*, 32(19):193001, feb 2020.
- [9] Takao Ohta. Active Matter and Its Non-linear Dynamics (akutibu mata no hisenkei dainamikusu, in Japanese). *BUT-*

- SURI*, 70(5):347–355, 2015.
- [10] Tamás Vicsek, András Czirók, Eshel Ben-Jacob, Inon Cohen, and Ofer Shochet. Novel Type of Phase Transition in a System of Self-Driven Particles. *Phys. Rev. Lett.*, 75:1226–1229, Aug 1995.
 - [11] John Toner and Yuhai Tu. Long-Range Order in a Two-Dimensional Dynamical XY Model: How Birds Fly Together. *Phys. Rev. Lett.*, 75:4326–4329, Dec 1995.
 - [12] John Toner and Yuhai Tu. Flocks, herds, and schools: A quantitative theory of flocking. *Phys. Rev. E*, 58:4828–4858, Oct 1998.
 - [13] H Chaté, F Ginelli, G Grégoire, F Peruani, and F Raynaud. Modeling collective motion: variations on the Vicsek model. *The European Physical Journal B*, 64(3):451–456, August 2008.
 - [14] M. E. Cates and J. Tailleur. When are active Brownian particles and run-and-tumble particles equivalent? Consequences for motility-induced phase separation. *Europhysics Letters*, 101(2):20010, feb 2013.
 - [15] Michael E. Cates and Julien Tailleur. Motility-Induced Phase Separation. *Annual Review of Condensed Matter Physics*, 6(1):219–244, 2015, <https://doi.org/10.1146/annurev-conmatphys-031214-014710>.
 - [16] Kazuki Sone, Yuto Ashida, and Takahiro Sagawa. Exceptional non-Hermitian topological edge mode and its application to active matter. *Nature Communications*, 11(1):5745, November 2020.
 - [17] Vijay Narayan, Sriram Ramaswamy, and Narayanan Menon. Long-Lived Giant Number Fluctuations in a Swarming Granular Nematic. *Science*, 317(5834):105–108, 2007, <https://www.science.org/doi/pdf/10.1126/science.1140414>.
 - [18] H. P. Zhang, Avraham Be’er, E.-L. Florin, and Harry L. Swinney. Collective motion and density fluctuations in bacterial colonies. *Proceedings of the National Academy of Sciences*, 107(31):13626–13630, 2010, <https://www.pnas.org/doi/pdf/10.1073/pnas.1001651107>.
 - [19] Gabriel S. Redner, Michael F. Hagan, and Aparna Baskaran. Structure and Dynamics of a Phase-Separating Active Colloidal Fluid. *Phys. Rev. Lett.*, 110:055701, Jan 2013.
 - [20] Kyogo Kawaguchi, Ryoichiro Kageyama, and Masaki Sano. Topological defects control collective dynamics in neural progenitor cell cultures. *Nature*, 545(7654):327–331, May 2017.
 - [21] Daiki Nishiguchi, Igor S Aranson, Alexey Snezhko, and Andrey Sokolov. Engineering bacterial vortex lattice via direct laser lithography. *Nature Communications*, 9(1):4486, October 2018.
 - [22] Kyosuke Adachi, Kazuaki Takasan, and Kyogo Kawaguchi. Activity-induced phase transition in a quantum many-body system. *Phys. Rev. Research*, 4:013194, Mar 2022.
 - [23] Yuanjian Zheng and Hartmut Löwen. A quantum active particle, 2023, 2305.16131.
 - [24] Kazuaki Takasan, Kyosuke Adachi, and Kyogo Kawaguchi. Activity-induced ferromagnetism in one-dimensional quantum many-body systems, 2023, 2308.04382.
 - [25] Reyhaneh Khasseh, Sascha Wald, Roderich Moessner, Christoph A. Weber, and Markus Heyl. Active quantum flocks, 2023, 2308.01603.
 - [26] Y. Aharonov, L. Davidovich, and N. Zagury. Quantum random walks. *Phys. Rev. A*, 48:1687–1690, Aug 1993.
 - [27] David A Meyer. From quantum cellular automata to quantum lattice gases. *Journal of Statistical Physics*, 85(5):551–574, December 1996.
 - [28] Edward Farhi and Sam Gutmann. Quantum computation and decision trees. *Phys. Rev. A*, 58:915–928, Aug 1998.
 - [29] Andris Ambainis, Eric Bach, Ashwin Nayak, Ashvin Vishwanath, and John Watrous. One-Dimensional Quantum Walks. In *Proceedings of the Thirty-Third Annual ACM Symposium on Theory of Computing*, STOC ’01, pages 37–49, New York, NY, USA, 2001. Association for Computing Machinery.
 - [30] Ryo Asaka, Kazumitsu Sakai, and Ryoko Yahagi. Quantum random access memory via quantum walk. *Quantum Science and Technology*, 6(3):035004, may 2021.
 - [31] Ali Mostafazadeh. Pseudo-Hermiticity versus PT symmetry: The necessary condition for the reality of the spectrum of a non-Hermitian Hamiltonian. *Journal of Mathematical Physics*, 43(1):205–214, 01 2002, https://pubs.aip.org/aip/jmp/article-pdf/43/1/205/7481018/205.1_online.pdf.
 - [32] Ali Mostafazadeh. Pseudo-Hermiticity versus PT-symmetry. II. A complete characterization of non-Hermitian Hamiltonians with a real spectrum. *Journal of Mathematical Physics*, 43(5):2814–2816, 04 2002, https://pubs.aip.org/aip/jmp/article-pdf/43/5/2814/8171928/2814.1_online.pdf.
 - [33] Ali Mostafazadeh. Pseudo-Hermiticity versus PT-symmetry III: Equivalence of pseudo-Hermiticity and the presence of antilinear symmetries. *Journal of Mathematical Physics*, 43(8):3944–3951, 07 2002, https://pubs.aip.org/aip/jmp/article-pdf/43/8/3944/8171918/3944.1_online.pdf.
 - [34] Vittorio Gorini, Andrzej Kossakowski, and E. C. G. Sudarshan. Completely Positive Dynamical Semigroups of N Level Systems. *J. Math. Phys.*, 17:821, 1976.
 - [35] G. Lindblad. On the generators of quantum dynamical semigroups. *Communications in Mathematical Physics*, 48(2):119–130, 1976.
 - [36] Herwig Ott. Single atom detection in ultracold quantum gases: a review of current progress. *Reports on Progress in Physics*, 79(5):054401, apr 2016.
 - [37] Yuto Ashida, Shunsuke Furukawa, and Masahito Ueda. Quantum critical behavior influenced by measurement backaction in ultracold gases. *Phys. Rev. A*, 94:053615, Nov 2016.
 - [38] Yuto Ashida, Shunsuke Furukawa, and Masahito Ueda. Parity-time-symmetric quantum critical phenomena. *Nature Communications*, 8(1):15791, 2017.
 - [39] Yuto Ashida, Zongping Gong, and Masahito Ueda. Non-hermitian physics. *Advances in Physics*, 69(3):249–435, 2020, <https://doi.org/10.1080/00018732.2021.1876991>.
 - [40] Masaya Nakagawa, Naoto Tsuji, Norio Kawakami, and Masahito Ueda. Dynamical sign reversal of magnetic correlations in dissipative hubbard models. *Phys. Rev. Lett.*, 124:147203, Apr 2020.
 - [41] M. Naghiloo, M. Abbasi, Yogesh N. Joglekar, and K. W. Murch. Quantum state tomography across the exceptional point in a single dissipative qubit. *Nature Physics*, 15(12):1232–1236, 2019.
 - [42] Weijian Chen, Maryam Abbasi, Yogesh N. Joglekar, and Kater W. Murch. Quantum jumps in the non-hermitian dynamics of a superconducting qubit. *Phys. Rev. Lett.*, 127:140504, Sep 2021.
 - [43] Lutz Schimansky-Geier, Werner Ebeling, and Udo Erdmann. Stationary Distribution Densities of Active Brownian Particles. *Acta Physica Polonica B - ACTA PHYS POL B*, 36, 05 2005.
 - [44] Jonathan R. Howse, Richard A. L. Jones, Anthony J. Ryan, Tim Gough, Reza Vafabakhsh, and Ramin Golestanian. Self-Motile Colloidal Particles: From Directed Propulsion to Random Walk. *Phys. Rev. Lett.*, 99:048102, Jul 2007.
 - [45] Walter F Paxton, Kevin C Kistler, Christine C Olmeda, Ayushman Sen, Sarah K St. Angelo, Yanyan Cao, Thomas E Mallouk, Paul E Lammert, and Vincent H Crespi. Catalytic Nanomotors: Autonomous Movement of Striped Nanorods. *J. Am. Chem. Soc.*, 126(41):13424–13431, October 2004.

- [46] Ken Mochizuki, Dakyeong Kim, and Hideaki Obuse. Explicit definition of \mathcal{PT} symmetry for nonunitary quantum walks with gain and loss. *Phys. Rev. A*, 93:062116, Jun 2016.
- [47] L Xiao, X Zhan, Z H Bian, K K Wang, X Zhang, X P Wang, J Li, K Mochizuki, D Kim, N Kawakami, W Yi, H Obuse, B C Sanders, and P Xue. Observation of topological edge states in parity-time-symmetric quantum walks. *Nature Physics*, 13(11):1117–1123, November 2017.
- [48] Naomichi Hatano and Hideaki Obuse. Delocalization of a non-hermitian quantum walk on random media in one dimension. *Annals of Physics*, 435:168615, 2021. Special Issue on Localisation 2020.
- [49] Richard Phillips Feynman and Albert Roach Hibbs. *Quantum mechanics and path integrals*. International series in pure and applied physics. McGraw-Hill, New York, NY, 1965.
- [50] Gregory S Engel, Tessa R Calhoun, Elizabeth L Read, Tae-Kyu Ahn, Tomáš Mančal, Yuan-Chung Cheng, Robert E Blankenship, and Graham R Fleming. Evidence for wavelike energy transfer through quantum coherence in photosynthetic systems. *Nature*, 446(7137):782–786, April 2007.
- [51] Naini Dudhe, Pratyush Kumar Sahoo, and Colin Benjamin. Testing quantum speedups in exciton transport through a photosynthetic complex using quantum stochastic walks. *Phys. Chem. Chem. Phys.*, 24:2601–2613, 2022.
- [52] Takashi Oka, Norio Konno, Ryotaro Arita, and Hideo Aoki. Breakdown of an Electric-Field Driven System: A Mapping to a Quantum Walk. *Phys. Rev. Lett.*, 94:100602, Mar 2005.
- [53] Takuya Kitagawa, Mark S. Rudner, Erez Berg, and Eugene Demler. Exploring topological phases with quantum walks. *Phys. Rev. A*, 82:033429, Sep 2010.
- [54] Hideaki Obuse and Norio Kawakami. Topological phases and delocalization of quantum walks in random environments. *Phys. Rev. B*, 84:195139, Nov 2011.
- [55] Takuya Kitagawa. Topological phenomena in quantum walks: elementary introduction to the physics of topological phases. *Quantum Information Processing*, 11(5):1107–1148, October 2012.
- [56] János K. Asbóth and Hideaki Obuse. Bulk-boundary correspondence for chiral symmetric quantum walks. *Phys. Rev. B*, 88:121406, Sep 2013.
- [57] Manami Yamagishi, Naomichi Hatano, Ken-Ichiro Imura, and Hideaki Obuse. Proposal of multidimensional quantum walks to explore Dirac and Schrödinger systems. *Phys. Rev. A*, 107:042206, Apr 2023.
- [58] Naomichi Hatano and David R. Nelson. Localization Transitions in Non-Hermitian Quantum Mechanics. *Phys. Rev. Lett.*, 77:570–573, Jul 1996.
- [59] Naomichi Hatano and David R. Nelson. Vortex pinning and non-Hermitian quantum mechanics. *Phys. Rev. B*, 56:8651–8673, Oct 1997.
- [60] Ali Mostafazadeh. Pseudounitary operators and pseudounitary quantum dynamics. *Journal of Mathematical Physics*, 45(3):932–946, 02 2004, https://pubs.aip.org/aip/jmp/article-pdf/45/3/932/8173225/932.1_online.pdf.
- [61] H Haken. *Waves, Photons, Atoms: Volume I*. Light. North-Holland, Oxford, England, December 1980.
- [62] Gerard Meurant and H Haken. *Laser light dynamics: Volume II*. Light. North-Holland, Oxford, England, February 1985.
- [63] Eiichi Hanamura. *Iwanami Lectures of Modern Physics: vol. 8 Quantum Optics (Iwanami kouza gendai no butsurigaku: vol. 8 ryoushi kougaku, in Japanese)*. Iwanami shoten, Tokyo, Japan, May 1992.
- [64] A. Kempf and R. Portugal. Group velocity of discrete-time quantum walks. *Phys. Rev. A*, 79:052317, May 2009.
- [65] R. Jackiw and C. Rebbi. Solitons with fermion number $\frac{1}{2}$. *Phys. Rev. D*, 13:3398–3409, Jun 1976.
- [66] Samuel Muga, Alessio Celi, Pietro Massignan, János K. Asbóth, Maciej Lewenstein, and Carlos Lobo. Topological bound states of a quantum walk with cold atoms. *Phys. Rev. A*, 94:023631, Aug 2016.
- [67] A. Schreiber, K. N. Cassemiro, V. Potoček, A. Gábris, P. J. Mosley, E. Andersson, I. Jex, and Ch. Silberhorn. Photons Walking the Line: A Quantum Walk with Adjustable Coin Operations. *Phys. Rev. Lett.*, 104:050502, Feb 2010.
- [68] Qi-Ping Su, Yu Zhang, Li Yu, Jia-Qi Zhou, Jin-Shuang Jin, Xiao-Qiang Xu, Shao-Jie Xiong, Qingjun Xu, Zhe Sun, Kefei Chen, Franco Nori, and Chui-Ping Yang. Experimental demonstration of quantum walks with initial superposition states. *npj Quantum Information*, 5(1):40, May 2019.
- [69] Zhiguang Yan, Yu-Ran Zhang, Ming Gong, Yulin Wu, Yaru Zheng, Shaowei Li, Can Wang, Futian Liang, Jin Lin, Yu Xu, Cheng Guo, Lihua Sun, Cheng-Zhi Peng, Keyu Xia, Hui Deng, Hao Rong, J. Q. You, Franco Nori, Heng Fan, Xiaobo Zhu, and Jian-Wei Pan. Strongly correlated quantum walks with a 12-qubit superconducting processor. *Science*, 364(6442):753–756, 2019, <https://www.science.org/doi/pdf/10.1126/science.aaw1611>.
- [70] Kohei Kawabata. Private communication. Comment on the use of the left-eigenvector and the Hermitian conjugate of the right-eigenvector., December 2018.
- [71] Naomichi Hatano. What is the resonant state in open quantum systems? *Journal of Physics: Conference Series*, 2038(1):012013, oct 2021.
- [72] Carl M. Bender and Stefan Boettcher. Real Spectra in Non-Hermitian Hamiltonians Having PT Symmetry. *Phys. Rev. Lett.*, 80:5243–5246, Jun 1998.
- [73] Carl M. Bender, Dorje C. Brody, and Hugh F. Jones. Complex Extension of Quantum Mechanics. *Phys. Rev. Lett.*, 89:270401, Dec 2002.